BARC/2014/E/016

BARC/2014/E/016

EXPERIMENTAL AND THEORETICAL STUDIES IN MOLTEN SALT NATURAL CIRCULATION LOOP (MSNCL)

by
A.K. Srivastava, A. Borgohain, S.S. Jana, R.K. Bagul, R.R. Singh, N.K. Maheshwari, D.G. Belokar and P.K. Vijayan
Reactor Engineering Division

BARC/2014/E/016

BARC/2014/E/016

GOVERNMENT OF INDIA
ATOMIC ENERGY COMMISSION

EXPERIMENTAL AND THEORETICAL STUDIES IN MOLTEN SALT NATURAL CIRCULATION LOOP (MSNCL)

by

A.K. Srivastava, A. Borgohain, S.S. Jana, R.K. Bagul, R.R. Singh, N.K. Maheshwari, D.G. Belokar and P.K. Vijayan
Reactor Engineering Division

BHABHA ATOMIC RESEARCH CENTRE
MUMBAI, INDIA
2014

BIBLIOGRAPHIC DESCRIPTION SHEET FOR TECHNICAL REPORT
(as per IS : 9400 - 1980)

01	*Security classification :*	Unclassified
02	*Distribution :*	External
03	*Report status :*	New
04	*Series :*	BARC External
05	*Report type :*	Technical Report
06	*Report No. :*	BARC/2014/E/016
07	*Part No. or Volume No. :*	
08	*Contract No. :*	
10	*Title and subtitle :*	Experimental and theoretical studies in Molten Salt Natural Circulation Loop (MSNCL)
11	*Collation :*	79 p., 23 figs., 8 tabs., 3 ills.
13	*Project No. :*	
20	*Personal author(s) :*	A.K. Srivastava; A. Borgohain; S.S. Jana; R.K. Bagul; R.R. Singh; N.K. Maheshwari; D.G. Belokar; P.K. Vijayan
21	*Affiliation of author(s) :*	Reactor Engineering Division, Bhabha Atomic Research Centre, Mumbai
22	Corporate author(s) :	Bhabha Atomic Research Centre, Mumbai - 400 085
23	*Originating unit :*	Reactor Engineering Division, Bhabha Atomic Research Centre, Mumbai
24	*Sponsor(s) Name :*	Department of Atomic Energy
	Type :	Government

Contd...

30	*Date of submission :*	November 2014
31	*Publication/Issue date :*	December 2014
40	*Publisher/Distributor :*	Head, Scientific Information Resource Division, Bhabha Atomic Research Centre, Mumbai
42	*Form of distribution :*	Hard copy
50	*Language of text :*	English
51	*Language of summary :*	English
52	*No. of references :*	21 refs.
53	*Gives data on :*	

60 *Abstract :* High Temperature Reactors (HTR) and solar thermal power plants use molten salt as a coolant, as it has low melting point and high boiling point, enabling us to operate the system at low pressure. Molten fluoride salt and molten nitrate salt are proposed as a candidate coolant for High Temperature Reactors (HTR) and solar power plant respectively. BARC is developing a 600 MW_{th} pebble bed high temperature reactor, cooled by natural circulation of fluoride salt and capable of supplying process heat at 1000°C to facilitate hydrogen production by splitting water. Beside this, BARC is also developing a 2MWe solar power tower system using molten nitrate salt. With these requirements, a Molten Salt Natural Circulation Loop (MSNCL) has been designed, fabricated, installed and commissioned in Hall-7, BARC for thermal hydraulic, instrumentation development and material compatibility related studies. Steady state natural circulation experiments with molten nitrate salt (mixture of $NaNO_3$ and KNO_3 in 60:40 ratio) have been carried out in the loop at different power level. Various transients viz. startup of natural circulation, step power change, loss of heat sink and heater trip has also been studied in the loop. A well known steady state correlation given by Vijayan et. al. has been compared with experimental data. In-house developed code LeBENC has also been validated against all steady state and transient experimental results. The detailed description of MSNCL, steady state and transient experimental results and validation of in-house developed code LeBENC have been described in this report

70	*Keywords/Descriptors :*	HTTR REACTOR; MOLTEN SALTS; COOLANT LOOPS; DESIGN; SOLAR THERMAL POWER PLANTS; REACTOR SAFETY; NATURAL CONVECTION
71	*INIS Subject Category :*	S21
99	*Supplementary elements :*	

ABSTRACT

High Temperature Reactors (HTR) and solar thermal power plants use molten salt as a coolant, as it has low melting point and high boiling point, enabling us to operate the system at low pressure. Molten fluoride salt and molten nitrate salt are proposed as a candidate coolant for High Temperature Reactors (HTR) and solar power plant respectively. BARC is developing a 600 MW_{th} pebble bed high temperature reactor, cooled by natural circulation of fluoride salt and capable of supplying process heat at 1000^{o}C to facilitate hydrogen production by splitting water. Beside this, BARC is also developing a 2MWe solar power tower system using molten nitrate salt. With these requirements, a Molten Salt Natural Circulation Loop (MSNCL) has been designed, fabricated, installed and commissioned in Hall-7, BARC for thermal hydraulic, instrumentation development and material compatibility related studies. Steady state natural circulation experiments with molten nitrate salt (mixture of $NaNO_3$ and KNO_3 in 60:40 ratio) have been carried out in the loop at different power level. Various transients viz. startup of natural circulation, step power change, loss of heat sink and heater trip has also been studied in the loop. A well known steady state correlation given by Vijayan et. al. has been compared with experimental data. In-house developed code LeBENC has also been validated against all steady state and transient experimental results. The detailed description of MSNCL, steady state and transient experimental results and validation of in-house developed code LeBENC have been described in this report.

CONTENTS

1. INTRODUCTION

In modern times, when each day we keep wondering at the newest technological advances, we are also reminded of the fact that the driving forces of most of these wonders are still now some or the other sources of non- renewable energy. And then we realize the importance of the quote, “offer valid till stocks last”. In such a scenario renewable and clean resources like solar and nuclear energies are a savior. But to use them in an effective manner is a challenge and requires the regular supply of some basic components. One such major requirement is the coolant and, molten salts have been unanimously accepted for this purpose in both solar power plants and high temperature nuclear reactors.

1.1 Molten salt Application to Solar Power and High-temperature Reactors

1.1.1 Solar Power

India is a tropical country abundant in solar insolation, which is available almost throughout the year more or less in the entire country. With increasing demand on fossil fuel reserves, poor quality of coal, increasing coal transportation and electricity transmission costs to longer distances, with its associated ecological impact and international community's pressure to reduce environmental pollution hazards, harnessing of solar energy, available in abundance for useful purposes, assumes significance.

Solar power is the conversion of sunlight into electricity. Sunlight can be converted directly into electricity using photovoltaic (PV), or indirectly by concentrating solar rays and focusing it on a receiver to generate steam which finally can be converted to electrical power through steam turbine and generator. A distinct advantage of solar thermal power plants compared with other renewable energies, such as photovoltaic’s (PV) and wind, is the possibility of using relatively cheap storage systems. That is, storing the thermal energy itself. Storing electricity is much more expensive.

Solar power is a predictably intermittent energy source, meaning that whilst solar power is not available at all times, we can predict with a very good degree of accuracy when it will and will not be available. Technologies such as solar thermal concentrators, with thermal storage such as molten salts can deliver heat at temperatures compatible with conventional power

systems, have the potential to eliminate the intermittency of solar power, by storing spare solar power in the form of heat; and using this heat overnight or during periods that solar power is not available to produce electricity. This technology has the potential to make solar power "dispatchable", as the heat source can be used to generate electricity at will.

Concentrated solar thermal (CST) power plants have emerged as one of the promising energy sources for generating electricity and mitigating the energy crisis in near future. CST power plant uses a field of sun tracking mirrors, called heliostats; to concentrate sunlight onto a tower mounted, centrally located receiver, where the thermal energy is collected into a heated fluid. Schematic of such system is shown in Fig. 1.

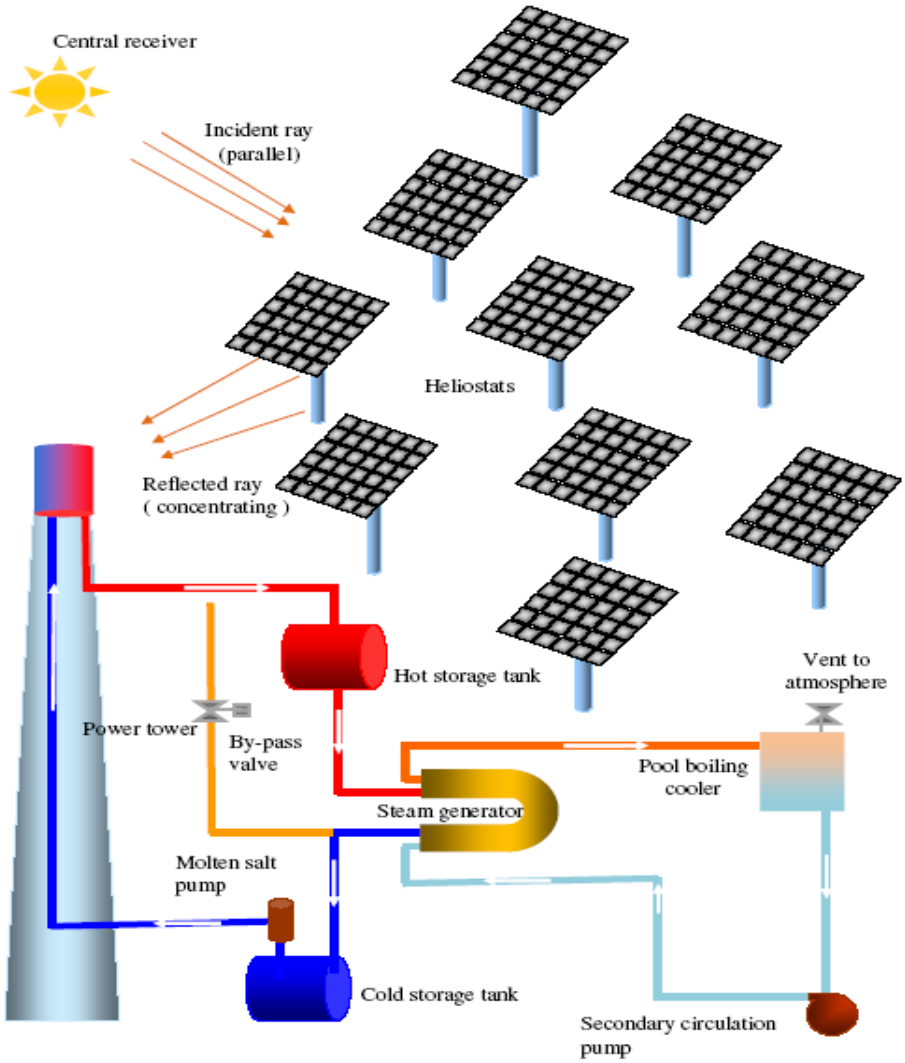

Figure 1 Schematic of molten salt based CST Power Plants

Thermal energy storage is critical for such systems so as to deliver electricity at the highest demand rates without any backup. Solar thermal energy in such systems is collected and delivered via a heat transfer fluid to a steam generator; this in turn drives the turbine for electricity production. Choice of heat storage-transfer medium is critical for proper operation of CST power plant.

High temperature solar thermal power plants use **Molten Salt** as a coolant and thermal storage medium, as it has low melting point and high boiling point, enabling us to operate the system at low pressure. There are number of coolants available for solar application. A few of them are listed below in table.1 [1].

Table 1. Coolants available for solar application

Coolant	**Melting point (^oC)**	**Maximum temperature upto which it can be used (^oC)**	**Avg. density (kg/m^3)**	**Average thermal conductivity (W/ mK)**	**Average heat capacity (kJ/kgK)**	**Cost** [1] **(Rs/kg)**
Mineral Oil	_	200	770	0.12	2.6	12
Synthetic oil	_	250	900	0.11	2.3	120
Silicone oil	_	300	900	0.1	2.1	200
Nitrite salts	124	500	1825	0.57	1.5	40
Nitrate salts	221	600	1870	0.52	1.6	30
Carbonate salts	450	750	2100	2.0	1.8	96

There are numerous salt compositions that can be considered for use. However, the nitrates of sodium and potassium can be shown to be of greatest interest by virtue of straight forward reasoning as follows: of the common salts sulfates and phosphates are too corrosive and the

melting points of the carbonates and fluorides are too high. One is left with nitrates, chlorides and bromides to choose from. Based upon cost and availability, the alkali metal nitrates appear to have the best chance for success in solar thermal large power systems. Molten salt, consisting of a mixture of $NaNO_3$ and KNO_3 in 60:40 ratio, is normally used in solar power plants.

Nitrate salts have been used for years in the chemicals and metal industries. The nitrate salt composition most commonly used is the three component mixture of KNO_3-$NaNO_2$-$NaNO_3$ in 53%-40%-7% ratio (by weight) respectively. This mixture is marketed commercially under the name HITEC by coastal chemicals and Partherm 290 by Park Chemical [2]. The nitrite constituent of this ternary mixture is not stable in air at temperatures greater than 500^{o}C; the nitrite is oxidized to form nitrate. Therefore compositions of interest for solar power systems which will see temperatures up to 600^{o}C in an air environment are found in the $NaNO_3$-KNO_3 binary. Draw salt is one such mixture. Draw salt is nominally an equimolar mixture of $NaNO_3$ and KNO_3, and was developed historically for high temperature metal treating baths. Due to cost consideration it is desirable to use a maximum of the less expensive $NaNO_3$ constituent. Therefore, off eutectic $NaNO_3$ rich compositions such as Partherm 430 marketed by Park Chemicals (60% NaNO3 – 40% KNO_3) are the salt compositions currently finding the greatest interest. A key issue is the thermal stability of the nitrate salts. Ideally the salt should be inert to degradation and chemical changes for the duration of the plant life (25-30 years). Nitrate salts have been the object of several studies, but a complete and unambiguous understanding of salt behavior at temperature of 600^{o}C does not yet exist. It is often assumed that the only important reaction is the nitrate-nitrite–oxygen equilibrium:

$$\text{Nitrate} \rightleftharpoons \text{Nitrite} + \text{Oxygen}$$

Another issue concerns the chemical reactivity of the salt with the gaseous environment. Nitrates react with CO_2 and H_2O in the atmosphere. The reaction with latter may not be a serious problem. H_2O apparently reacts reversibly with the salt. Water dilution systems have been developed and are marketed commercially. In these systems, water is added to the salt during shut down to lower the melting point. The water is driven off by raising the salt temperature and allowing the water to evaporate and escape from the system. These systems undergo many cycles of dilution and concentration without apparent degradation of the salt.

Interactions with CO_2 are, however, of greater concern. CO_2 reacts with the nitrate ions to form carbonate. Carbonate tends to precipitate out of the salt, and therefore pose two serious problems: first, solids may build-up in undesirable spots. Causing blockage of fluid flow and second, for every carbonate ion formed there is a loss of a nitrate ion. It has been suggested that carbonates can form only after the formation of the hydroxide species which results from salt-water interactions. Molten nitrate salt cooled solar power systems could be designed to eliminate contact with CO_2, perhaps by the use of gas scrubbing systems.

1.1.1.1 Thermophysical Properties of the Nitrate Salt

Table 2 shows the thermophysical properties of molten nitrate salt at 426^{o}C. The temperature dependent properties of molten nitrate salt are given in Appendix- 1.

Table 2. Thermophysical properties of molten nitrate salt

Salt	Specific heat (J/kgK)	Density (kg/m^3)	Thermal conductivity (W/mK)	Viscosity (Pa.s)	Prandtl No.
Nitrate salt mixture 60% $NaNO_3$ – 40% KNO_3 (by weight)	1520	1818	0.53	1.583E-03	4.58

1.1.1.2 Corrosion in nitrate salt environment

Investigations of the corrosion of various metals, alloys, and ceramics in high-temperature nitrate salt melts revealed that relatively few materials have acceptable compatibility at 600°C in $NaNO_3$ and KNO_3 environment [2]. Corrosion in these systems was controlled by the stabilities of the salt and solid-state surface oxides (whether they were pre-existing or formed upon exposure), the salt's oxide ion activity, and the physical condition of the solid surfaces.

To summarize the general corrosion results to date, Incoloy 800 is the conservative first choice alloy candidate for use in the 500-600^{o}C temperature range. As long as the temperature

does not exceed 600^{o}C, the uniform corrosion process appears to take the form of protective oxide formation. Above 600^{o}C undesirable processes become more pronounced, and results in Cr depletion.

1.1.1.3 Materials used in nitrate salt environment

Generally for application to nitrate salt environment: SS 304, and Carbon steel can be used up to 350^{o}C. For application to higher temperature up to 600^{o}C, SS 347, SS 321, SS 316, Incolloy 800, Hynes 242, Inconel 718, Inconel 625 can be used [2].

1.1.2 High Temperature Reactor (HTR)

Next generation high temperature reactors as needed for hydrogen production and similar other applications, will need to incorporate innovative approaches to further enhance their reliability and safety as needed for large scale deployment in different regions of the world. An important feature of these reactors will be the use of coolants at temperatures much higher than that being used in current generation reactors. Molten salts, liquid metals and supercritical fluids are being considered as potential coolants for core cooling of advanced nuclear reactors. In order to design reactors it is necessary to study the various coolants and characterize their thermal hydraulic performance in terms of heat transfer coefficients, pressure drops, etc. In high temperature reactors the process heat is required for hydrogen production at a nearly constant temperature. Gas-cooled (He, CO_2) reactors have several hundred degree temperature rises across the reactor core to minimize pumping power whereas liquid-cooled (supercritical water, liquid metal, molten salt) reactors have temperature rise of several tens of degrees. If heat is needed at 750^{o}C, the maximum temperature for the gas coolant may exceed 1000^{o}C and hence maximize high temperature material requirements. Whereas traditional liquid metals such as sodium (BP~883^{0}C) can not be used for high temperature operations because of their relatively low boiling points. Heavy liquid metals (molten lead or lead alloys) which have high boiling points can be used as high temperature coolants but they have a very high density. Supercritical fluids are high temperature and high pressure coolants. It draws our focus to design high pressure (~220 bars for water) reactor components. Therefore, Molten Salts, which can be used for high temperature (~1000^{o}C) at very low pressure (~1 atm), proved as potential candidate coolant for high temperature operation. Physical properties of various reactor coolants are listed in table 3.

Table 3. Properties of various coolants

Coolant	Melting point (^{O}C)	Boiling point (^{O}C)	Density (kg/m^3)	Sp. Heat (kJ/kg.^{O}C)	Thermal conductivity (W/mK)	Viscosity *10^5 (m^2/s)	Prandtl Number
Water (7.5MPa)	0	290	732	5.5	0.56	0.13	9.3
FLiNaK (Molten Salt)	454	1570	2020	1.81	1.0	0.15	5.65
Sodium	97.8	883	832	1.27	70	0.025	0.004
Lead-Bismuth eutectic	123	1670	10080	0.146	15	0.13	0.013
Helium	_	_	3.8	5.2	0.29	11.0	7.5

Fluorides are deemed as the most suitable molten salts, for their good nuclear properties, chemical stability and favorable thermo-physical properties. A large number of fluoride salts are available as candidate coolants for high temperature reactor. Some of them are listed below in table 4.

1.1.2.1 Chemistry of the molten fluoride salt coolants

I. Purity of molten salt

On line salt purification is required to prevent severe corrosion of container materials and other impurities.

II. Studies on Phase-Diagrams

Salt components (i.e. LiF, BeF_2 etc.) have high melting point (>800^{o}C) and that preclude their use as nuclear coolant. However the combination of the individual components can produce low-melting mixtures.

III. Acid-Base Chemistry

The salt coolant should not be highly acidic or basic in nature. An effective Redox buffer strategy is to be developed to maintain a non-corrosive environment in the coolant circuit.

The expansion during phase change of the molten salt may create excessive stress on the structural material.

Table 4. Proposed fluoride salt coolants for HTR

Salt	MP (^oC)	Vapour Pressure (mm of Hg)	Density (kg/m^3)	Volumetric heat capacity ($cal/cm^3\ ^oC$)	Viscosity (Ns/m^2)	Thermal conductivity (W/mK)	Mode-rating ratio	Neutron Capture relative to graphite
LiF-NaF-KF	454	~0.7	2020	0.91	0.0029	0.92	2	90
LiF-BeF_2	460	1.2	1940	1.12	0.0056	1.0	60	8
LiF-NaF-RbF	435	~0.8	2690	0.63	0.0026	0.62	8	20
LiF-NaF-BeF_2	315	1.7	2000	0.98	0.005	0.97	22	20
KF-ZrF_4	390	_	2800	0.70	<0.0051	0.45	3	67

IV. Phase Change of Salt

Proper melting and solidification strategy are needed to be developed during start up and shut down of the reactor. Development of molten salts with low or zero expansion coefficients during phase change is the most suitable solution.

1.1.2.2 Materials used in Fluoride Salt Environment

Generally for application to fluoride salt environment Inconel 617, Hestelloy N, Hynes 25, 263 and 188 can be used in a temperature range of 700 ^oC -930 ^oC. For further application to higher temperature up to 1100^oC- TZM Moly., Hynes 214 and Waspolloy can be used.

2. OBJECTIVES OF THIS STUDY

BARC is developing a 600 MW_{th} pebble bed high temperature reactor, cooled by natural circulation of fluoride salt and capable of supplying process heat at 1000^oC to facilitate hydrogen

production by splitting water. Beside this, BARC is also developing a $2MW_e$ solar power tower system using molten nitrate salt a primary coolant. In order to design this, it is necessary to study the thermal-hydraulic behaviour of various molten salts and compatibility of the same with available high temperature structural materials under different conditions. There is great interest in natural circulation flow of molten salt in various high temperature systems but very few experimental studies have been carried out so far. With this in view, a molten salt natural circulation test loop has been designed, fabricated, installed and commissioned in Hall-7, BARC with following objective:

i. Thermal Hydraulic and material related studies on molten salt.
ii. To determine pressure drop across various components in the loop.
iii. To develop high temperature instruments and test/calibrate them in the loop.
iv. To validate the design of various proposed components of CHTR and Solar power tower.
v. To validate computer code developed for natural circulation
vi. Development of intermediate heat exchanger for high temperature application

The experimentation program is divided in two phases. In the 1st phase the experimental studies with molten nitrate salt (mixture of $NaNO_3$ and KNO_3 in 60:40 ratio) has been performed. Experimental studies with different molten fluoride salts will be carried out in 2nd phase.

3. REVIEW OF PREVIOUS WORK

3.1 Heat transfer and fluid flow studies related to Molten salts

A literature review is performed to collect and analyze these data.

Hoffman and Lones [3] studied the compatibility of structural material for FLiNaK salt. They stated that Nickel will contain FLiNaK but is subjected to fatigue failure at temperature above 1000^oF. Therefore, Inconel, which exhibit good corrosion resistance to FLiNaK and retains its structural strength at elevated temperatures, was adapted as a material of construction. FLiNaK salt heat transfer study with different test section material was also performed and heat transfer data is generated. The experimental data was compared with Colburn j-function:

$$j = St.\mathrm{Pr}^{2/3} = 0.023\,\mathrm{Re}^{-0.2} \quad (1)$$

For FLiNaK-Inconel system, they observed a mismatch between experimental data and Eq. 1. The reason for mismatch of FLiNaK-Inconel systems was given as:

In the FLiNaK-Inconel system an insoluble, high-melting surface deposit (film) results from a reaction at the fluid-metal interface. The thermal resistance of this film is sufficient to cause a marked reduction in heat transfer for FLiNaK flowing in small diameter Inconel tubes. For this type of systems where deposits occur, knowledge of the thermal resistance of film is required.

Silverman et. al. [4] determined the heat transfer coefficient, experimentally, for two molten fluoride salts: [LiF-BeF_2-ThF_2-UF_4 (72-16-12-0.3 mole %)] and $NaBF_4$-NaF (92-8 mole %), proposed as the fuel salt and coolant salt, respectively, for molten salt breeder reactors. Information was obtained over a wide range of variables, with salt flowing through 12.7 mm OD Hastelloy N tubing in a forced convection loop. The heat transfer coefficient obtained experimentally was compared with the empirical correlation and found a satisfactory agreement with Sieder-Tate correlation in the fully developed turbulent region at Reynolds number above 15000, with a modified Hausen equation in the extended transition region (Re ~2100-15000). Insufficient data were obtained in the laminar region to allow any conclusion to be drawn.

Kearney et al. [5] investigated the feasibility of utilizing a molten slat as the heat transfer fluid and for thermal storage in a parabolic trough solar field to improve system performance and to reduce the levelized electricity cost. They mentioned: with salt, it may be possible to raise the solar field output temperature to 450-500^{o}C, thereby increasing the Rankine cycle efficiency of the power block steam turbine to the 40% range. This compares with the solar field outlet temperature cycle efficiency of 393^{o}C and 37.6%, respectively, for the current plant designs. The heat transfer fluid temperature rise in the collector field can increase up to a factor of 2.5, reducing the physical size of the thermal storage system for a given capacity. Moreover, molten salt is cheaper and more environmentally benign than the present heat transfer fluid. They suggested that protective heating systems for the solar field are necessary for start-up, maintenance, or to recover from a frozen condition brought about by an unexpected equipment outage.

Bradshaw& Siegel [6] identified a range of quaternary molten salt compositions, based on solar nitrate salt. That composition displays much lower liquidus temperature and they may be useful

for solar thermal energy systems. These molten salt mixtures contain calcium nitrate and lithium nitrate to depress the melting point of a salt mixture based on sodium nitrate and potassium nitrate. They experimentally established the working temperature ranges of these salt mixtures and concluded that these quaternary mixtures can be used up to a maximum temperature of 500^{o}C.

Yu-ting el al. [7] studied experimentally the forced convective heat transfer behavior of molten salt ($LiNO_3$) in laminar- turbulent transition region and generated a correlation based on experimental data:

$$Nu = 0.007(\mathrm{Re}^{0.92} - 280)\,\mathrm{Pr}^{0.4}\left[1+\left(\frac{d}{l}\right)^{2/3}\right]\left(\frac{\mathrm{Pr}_f}{\mathrm{Pr}_w}\right)^{0.11} \quad (2)$$

Equation 2 is valid for Reynolds number, Re ranging from 4100 to 9850 and Prandtl number ranging from 15.0 to 18.4.

This generated correlation is compared with the experimental data, Eq. 5 and Eq. 6 and found in a good agreement.

Hausen: $Nu = 0.037(\mathrm{Re}^{0.75} - 180)\,\mathrm{Pr}^{0.42}[1+(d/l)^{2/3}](\mu_b/\mu_w)^{0.14}$ (3)

Gnielinski: $Nu = 0.012(\mathrm{Re}^{0.87} - 280)\,\mathrm{Pr}^{0.4}[1+(d/l)^{2/3}](\mathrm{Pr}_b/\mathrm{Pr}_w)^{0.11}$ (4)

Liu et al. [8] performed experiments with molten salt ($LiNO_3$) in the Reynolds number range of 19,800 to 46,000. The Prandtl number of $LiNO_3$ is in the range 12.7 – 14.7. They used the well known convective heat transfer correlations by Hausen, Gnielinski, Dittus-Boelter and Sieder-Tate for comparing the results. These correlations are shown in Equations 3-6

Dittus-Boelter: $Nu = 0.023\,\mathrm{Re}^{0.8}\,\mathrm{Pr}^{n}$ where 0.3<n<0.4 (5)

Sieder-Tate: $Nu = 0.0242\,\mathrm{Re}^{0.81}\,\mathrm{Pr}^{0.333}(\mu_b/\mu_w)^{0.14}$ (6)

They studied the turbulent convective heat transfer with molten salt in a circular pipe and found a correlation for heat transfer based on their experiment in a forced convection loop. The correlation is:

$$Nu = 0.0242\,\mathrm{Re}^{0.81}\,\mathrm{Pr}^{1/3}\left(\frac{\mu_b}{\mu_w}\right)^{0.14} \quad (7)$$

The generated correlation is compared with the experimental results for $LiNO_3$ molten salt and stated that the correlation is valid in the range of Reynolds number 17000 to 45000 and Prandtl number 12.7 to 14.7.

Marcello et. al. [9] studied the thermal-hydraulic behavior of graphite-moderated channel type molten salt breeder reactor designed by ORNL. They had performed a preliminary study on heat transfer and pressure losses in typical MSR core channel and compared the results obtained using CFD code FLUENT and COMSOL.

3.2 Corrosion and material studies related to molten salt

Olson et. al. [10] had performed a corrosion test of high temperature alloys Hastelloy-N, Hastelloy-X, Haynes-230, Inconel-617, and Incoloy-800H in molten fluoride salt, FLiNaK (LiF–NaF–KF : 46.5–11.5–42 mol%) with the goal of understanding the corrosion mechanisms and ranking these alloys for their suitability for molten fluoride salt heat exchanger and thermal storage applications. The tests were performed at 850 ^oC for 500 hr in sealed graphite crucibles under an argon cover gas. Two chromium free alloys Ni-201 and Nb-1Zr were also tested and found that Ni-201 alloy, which is predominantly Ni with minor alloying additions, was resistant to corrosion. The refractory alloy Nb–1Zr exhibited severe corrosion and embrittlement.

Kaisar et.al. [11] studied the compatibility of SS 316 in ternary molten salt KNO_3-$NaNO_2$-$NaNO_3$ mixture and found that the corrosion rate of SS 316 is very much a function of temperature. He, finally concluded that this alloy should not be used at or above 550oC in ternary nitrate salt. An alternative, if this salt has to be used above 550oC more corrosion resistant alloy such as Hastellloy N should be used.

Baraka et. al. [12] has investigated the corrosion of nickel in molten $NaNO_3$-KNO_3 mixture at temperatures ranging from 250^oC to 450^oC for exposure period of upto 12 hrs. The results of both weight gain and potential measurements under open circuit conditions reveal the formation of passivating film consisting mainly of NiO. The thickening of the oxide film proceeds according to parabolic law at a rate depending on the temperature of the melt.

The influence of an oxidizing molten nitrate salt (60%NaNO3-40%KNO3) on the mechanical properties of 2.25Cr-1Mo has been examined by Goods [13] through a series of slow strain rate

tests at 450^{o}C and 550^{o}C. Two different environment-air and molten nitrate salt have been selected to check the susceptibility of the alloy to different environment by comparing fracture strain, reduction in area and ultimate strength.

3.3 Natural Circulation

Natural circulation is a simple phenomenon which occurs within a fluid in the presence of temperature and density gradients. In natural circulation systems there are a heat source and a heat sink, with the former placed lower than the later, both in contact with a portion of the fluid. As a consequence of the heat flux, the heated part of the fluid becomes lighter and rises up, while the cooled part becomes denser and is dropped down due to gravity. These combined effects establish circulation.

As it does not need any moving mechanical part, like pump or fan, natural circulation is characterized by high reliability and low costs of maintenance. On the other hand, the design of systems which use natural circulation as the primary heat transfer mechanism is very critical. This is because the thermal performances of the above system should to optimize and unwanted dynamic behavior, such as flow instabilities and flow reversals should be avoided.

Natural circulation loops are used in wide fields of engineering applications and are characterized by different sizes and attributes; in particular, they are employed in nuclear power generation, geothermal process, solar heaters, cooling of internal combustion engines and turbine blades.

In literature there are many reviews about single phase natural circulation:

Vijayan et al. [14] studied and compared the dynamic behavior of rectangular loop with different displacements of heater and cooler. They found out that the most stable configuration is the one with both vertical cooler and heater, which never present instability, while the common one with both heat exchangers on horizontal side, is less stable.

Zvirin [15] presented a survey on both theoretical and experimental works on natural circulation loops with modeling methods used to describe steady state flows, transients and stability characteristics.

Welander [16] proposed a model which consist a loop made by point heat source and point heat sink, both with imposed wall temperature, connected by two adiabatic legs. Welander explained

the presence of instabilities and flow reversal with the "hot pocket" theory: when buoyancy forces and shear stresses are not in phase, in case of specific boundary conditions, the presence of a temperature discontinuity (hot pocket) may cause an initial velocity oscillation, which grows in time and amplitude, eventually producing a flow reversal.

Tortorelli et al. [17] studied the corrosion of Fe-Ni-Cr alloys by draw salt (60% NaNO3 – 40% KNO_3 by wt.) with thermal convection loops of alloy 800 and type 304L and 316 stainless steel and concluded that 600^0C may be the limiting temperature for use of the above alloys in draw salt.

4. MOLTEN SALT NATURAL CIRCULATION LOOP (MSNCL)

4.1 General description of the loop

The experimental facility has been fabricated with ½" (15 NB) uniform diameter pipe (Figures 2-4). It has been designed to handle high temperature molten salt at various operating conditions. The loop has been designed in a way such that four different orientations of heater and cooler viz. Vertical Heater Vertical cooler (VHVC), Vertical Heater Horizontal Cooler (VHHC), Horizontal Heater Horizontal Cooler (HHHC) and Horizontal Heater Vertical Cooler (HHVC) can be analyzed. Any of the above combinations (HHHC, HHVC, VHVC or VHHC) can be chosen prior to the experiment. The primary fluid takes up heat in the heater section and on becoming lighter, it rises through the riser. It rejects heat in the cooler and on becoming heavier goes down the down comer and reaches heater inlet thereby establishing natural circulation. Initially, the salt powder was melted in the melt tank and then pressurized by argon gas system to fill the entire loop. On pressurization, the molten salt flowed into the loop and subsequently filled up the loop. When the loop was filled completely, it was isolated from the melt tank with the help of a control valve. Natural circulation took place by heating the molten salt in heater section and cooling it into the cooler section. Air has been used as a coolant in this loop. After cooling into the cooler section, the molten salt again entered into the heater section to maintain the continuous flow in the loop. High purity argon has been used as a cover gas in both the tanks. The instrumentation and control systems have been designed in such a way that the loop can be operated remotely as far as possible. An expansion tank has been provided at the highest elevation of the loop as shown in Fig. 2, Fig. 3 and Fig. 4 to accomodate thermal expansion of

the fluid. Band heaters have been provided for melting and keeping the salt at desired temperature in both the melt tank and expansion tank.

4.2 Design of the loop

4.2.1 Design Parameters of test facility

The loop design parameters have been listed in Table 5.

Table 5. Design Conditions of the Loop

Description	Operating Fluid	Material	Design Pressure (kgf/cm^2)	Design Temp. (^oC)
Main Loop	Molten nitrate salt ($NaNO_3$:KNO_3::60:40)	Inconel-625	5	800
Expansion Tank	Molten nitrate salt ($NaNO_3$:KNO_3::60:40)	SS 316	5	600
Melt Tank	Molten nitrate salt ($NaNO_3$:KNO_3::60:40)	SS 316	5	600

Operating parameter for MSNCL

- Maximum Operating Temperature = 565^oC
- Operating Pressure = 0.5 kgf/cm^2

4.2.2 Design of various components

Molten Salt Natural Circulation Loop (MSNCL) comprises five parts: heater, cooler, melt tank, expansion tank and main loop piping. The detailed design and specifications of the parts/components are as follows:

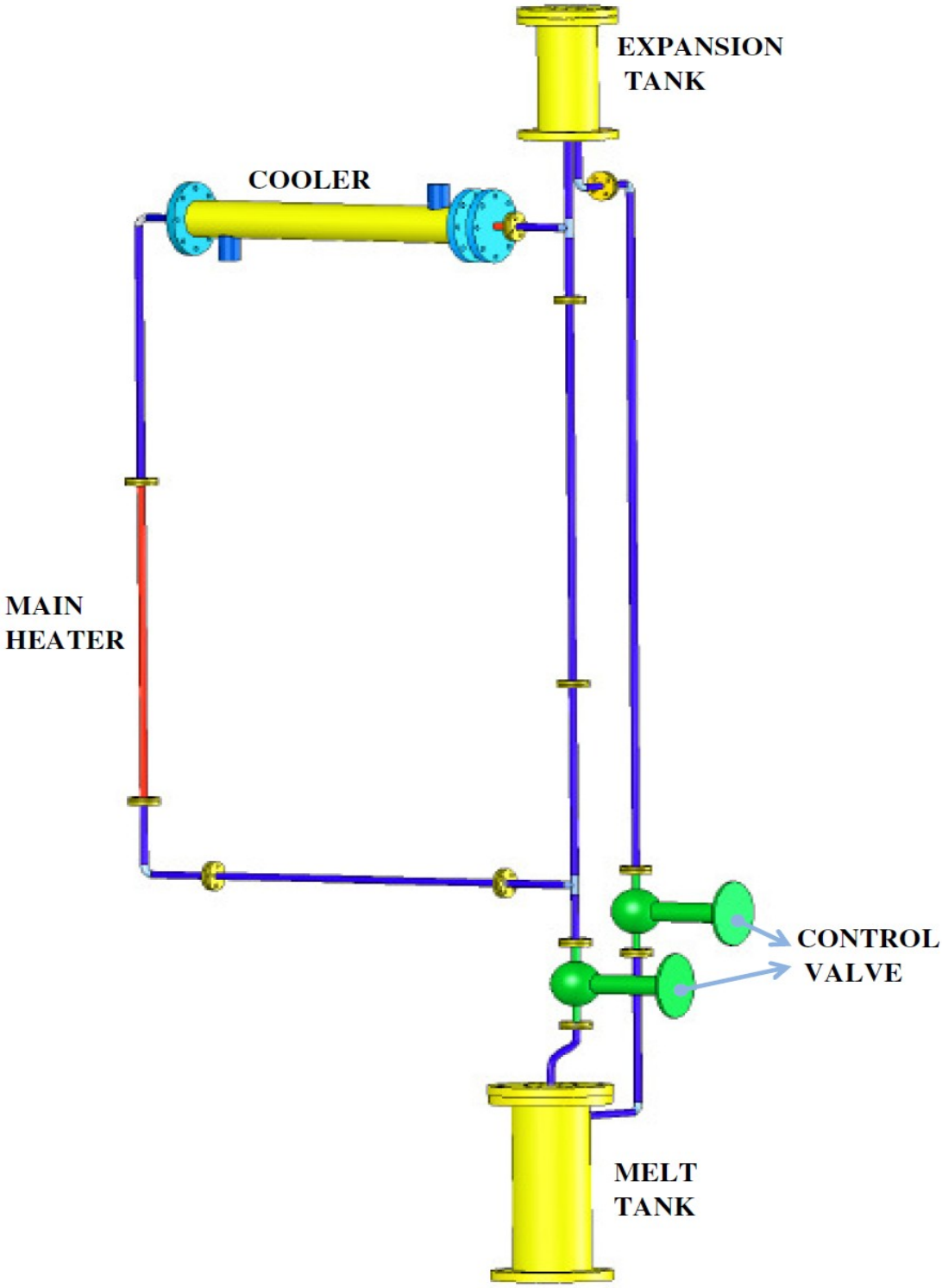

Figure 2. Isometric view of MSNCL

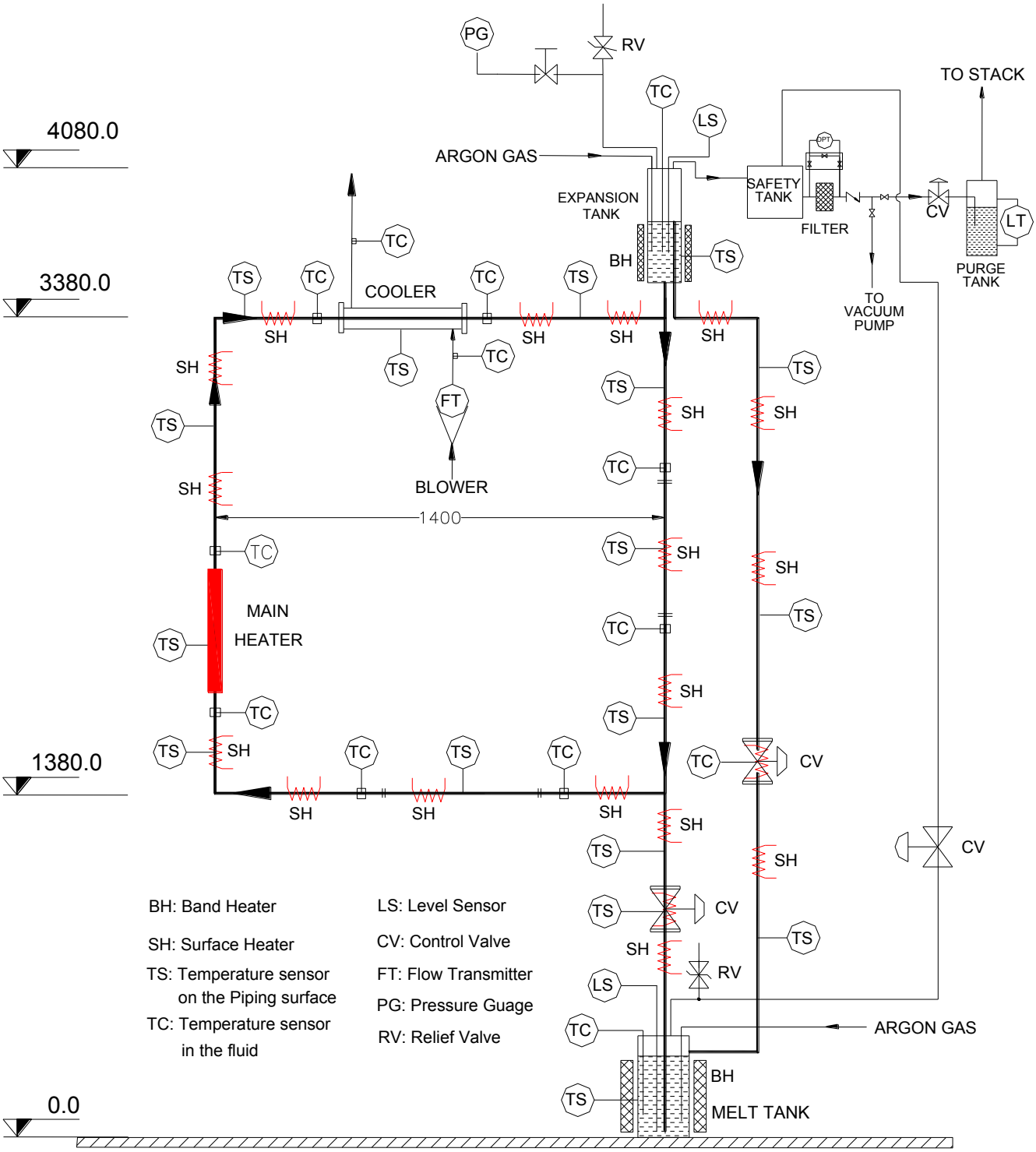

Figure 3. Flow sheet of MSNCL

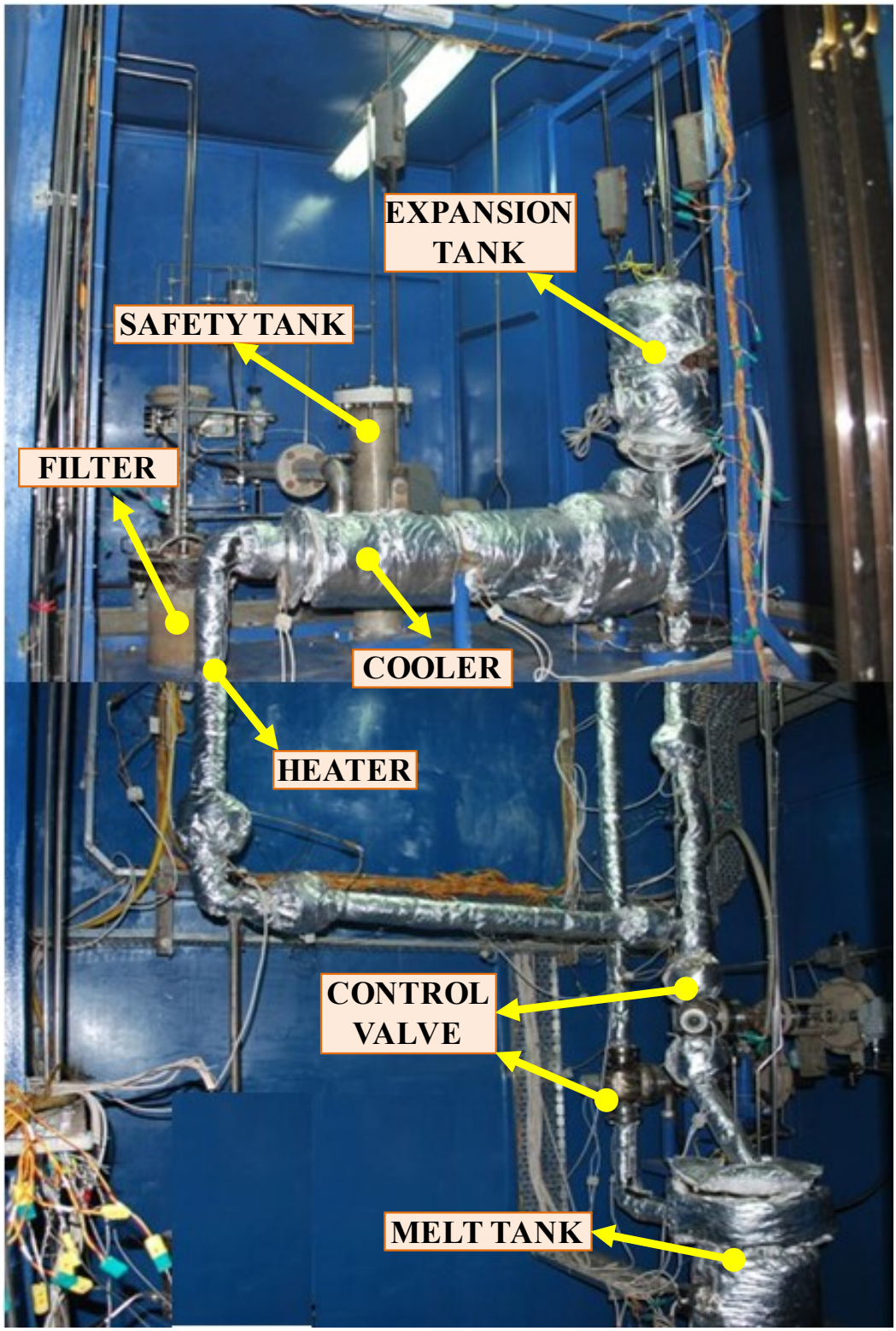

Figure 4. Photograph of MSNCL

I. Main Loop

The main loop is a ½" (ID=14 mm), uniform diameter, 2.0 m x 1.4 m rectangular loop. Inconel 625 is used as a material of loop piping. Coolers and heaters have been installed on the loop piping as shown in the Figure 3.

II. Melt Tank

The melt tank has been installed at the bottom of the loop. As the name indicates, salt is melted in this tank and with the help of the gas pressure; the molten salt is raised to fill the entire loop. It has been fabricated with SS316, 8" (200NB) SCH 40 (ID=202.74 mm), uniform diameter pipe with 500 mm height. The blind flange used to cover the top of the tank, have total 9 holes drilled for the instrumentation purpose.

III. Expansion Tank

The expansion tank is used to accommodate the volumetric expansion of the salt. The tank has been installed at the top of the loop as shown in Fig.1. It has been fabricated with SS316, 6" (150NB) SCH 40 (ID=153.96 mm) pipe having top blind flange drilled for instrumentation purpose. During experiment, half of the tank was filled with molten salt and half of it with cover gas.

4.3 Molten salt used

A mixture of sodium nitrate ($NaNO_3$) and potassium nitrate (KNO_3) in 60:40 ratio by weight has been used as working medium. Total Quantity of salt inventory inside the loop was 25 kg.

4.4 Blower

Air has been used as a cooling media in the secondary side of the loop. The cooling load of the cooler is 2.5kW. A separate blower has been attached to the loop for providing the air. To remove 2.5 kW of heat, 536 CFM flow rate was required from the blower. The specification of the blower is as follows:

Phase	: 3 Phase
Power	: 3HP
Maximum Flow	: 1000 CFM

4.5 Dimensions, Material specifications and ratings of Pipes, Flanges, Fittings and Gaskets

Socket welded piping components has been used in the molten salt loop. The detailed specification of that and their codal compliances has been listed here:

I. Pipe:

Sr. No.	Size	Specification	Material	Code
1	½”(15NB)	Schedule 80	Inconel 625	ASME B31.3
2	8” (200NB)	Schedule 40	SS 316	ASME B31.3
3	6” (150NB)	Schedule 40	SS 316	ASME B31.3
4	4”(100NB)	Schedule 40	SS 316	ASME B31.3

II. Flange:

Sr. No.	Size	Class	Type	Material	Code
1	½”(15NB)	300 LBS	SORF	Inconel 625	ASME B 16.5
2	½”(15NB)	300 LBS	SORF	SS 316	ASME B 16.5
3	8” (200NB)	150 LBS	SWRF	SS 316	ASME B 16.5
4	6” (150NB)	150 LBS	SWRF	SS 316	ASME B 16.5
5	4”(100NB)	150 LBS	SORF	SS 316	ASME B 16.5

III. Fittings and Gaskets

Sr. No.	Item	Size	Class	Type	Material	Code
1	90^0 Elbow	½”(15NB)	6000 LBS	Socket weld	Inconel 625	ASME B16.11
2	Equal Tee	½”(15NB)	6000 LBS	Socket weld	Inconel 625	ASME B16.11
3	Adapter	½”NPT	6000 LBS	Socket weld	SS 316	ASME B16.11
4	Gasket	½” (Spiral-Wound)	-	Metallic	Inconel 625	ASME B16.20
5	Gasket	8” (Spiral-Wound)	-	Metallic	SS 316	ASME B16.20
6	Gasket	6” (Spiral-Wound)	-	Metallic	SS 316	ASME B16.20

4.6 Piping Flexibility Analysis of MSNCL

The aim of the piping flexibility analysis of molten salt loop was to check the adequacy of support scheme under dead weight and thermal loads during operation. Flexibility analysis of MSNCL was carried out using CAESER II code.

4.6.1 CAESER II modeling

CAESER II is a standard piping stress analysis software. The piping model is generated through user interactive data spreadsheets. Input data includes geometrical details of piping layout, operating pressure and temperature, and piping restrains/supports. CAESER II iteratively solves the model to obtain the converged solutions for pipe stress and reactions at restraints. It also includes wide database for hanger selection for flexible supports. The stresses obtained can be checked against the piping standards such as ASME B31.3.

4.6.2 Flexibility Analysis of Molten Salt Natural Circulation Loop (MSNCL)

The CAESER II piping model for MSNCL has been prepared and support scheme has been analyzed to ascertain the piping stress do comply allowable limits described by ASME B31.3 standard. Figure 5 shows the CAESER II model of MSNCL. All the parts of the loop such as melt tank, expansion tank, cooler, valves etc has been modeled. The outlet of the cooler has not been modeled as it is free to move in all directions so it can not pose any resistance to movement. The cooler has been modeled in such a way that its one end is free to move axially to accommodate thermal expansion. The piping model connecting different loop components comprised number of pipe elements and nodes. CEASER II allows pipe material input from the available data base, thus the material constants have been used from its standard material database. The database for main loop piping material i.e. Inconel 625, was not available. Hence the required data for Inconel 625 has been incorporated in the CEASER II from ASME B31.3 code. The pressure and temperature conditions were taken as 500 kPa and 600^{o}C respectively.

Figure 6 shows the support scheme considered for the piping layout of the MSNCL. The support scheme has been devised after several trial runs and checking the piping stresses against the standards. The two control valves and the inlet pipe of the cooler has been taken as rigid support/anchors. A variable spring hanger has been provided to support the expansion tank and the cooler. The software selects the appropriate hanger from the database from various manufacturers. In our case SARATHI, make spring has been selected for the database to choose the hanger. A compression spring support has been given to the melt tank and a simply support has been provided at one end on the bottom horizontal leg.

Flexibility analysis consists of calculation of pipe stresses for the following load cases:

I. *Sustained Load case*: The dead weight of the piping, rigid elements (flanges, Valves etc.) and fluid inside the loop have been considered as loading to calculate the pipe stresses.

II. *Operating Load case*: Thermal loading along with the loads in above case have been considered for calculating the pipe stresses.

III. *Expansion Load case:* thermal stresses generated due to constraints on expansions of pipes have been calculated in this load case.

The allowable limits on the stresses for the sustained load and expansion load cases were governed by the piping code. CAESER II compares the calculated stresses with the allowable limit prescribed by the code ASME B 31.3. The operating stresses calculated by CAESER II code has to be assessed by the user/designer.

CAESER II also generates a hanger design load case to select the flexible support if the design is not specified by the user. In this case; the spring hangers were available to us. Those hangers have been used in the loop and the same has been used for the analysis of the stresses. CAESER II also generates a hanger design load case to select the flexible support if the design is not specified by the user.

The flexibility analysis for the given support scheme and pressure temperature loads as mentioned earlier has been carried out and it has been found that the sustained and expansion load case stresses do not exceed the allowable stresses limit provided by the piping code ASME B 31.3. The maximum stress calculated by CAESER II and the allowable stresses provided by the ASME B 31.3 for different loading cases are listed in Table 6:

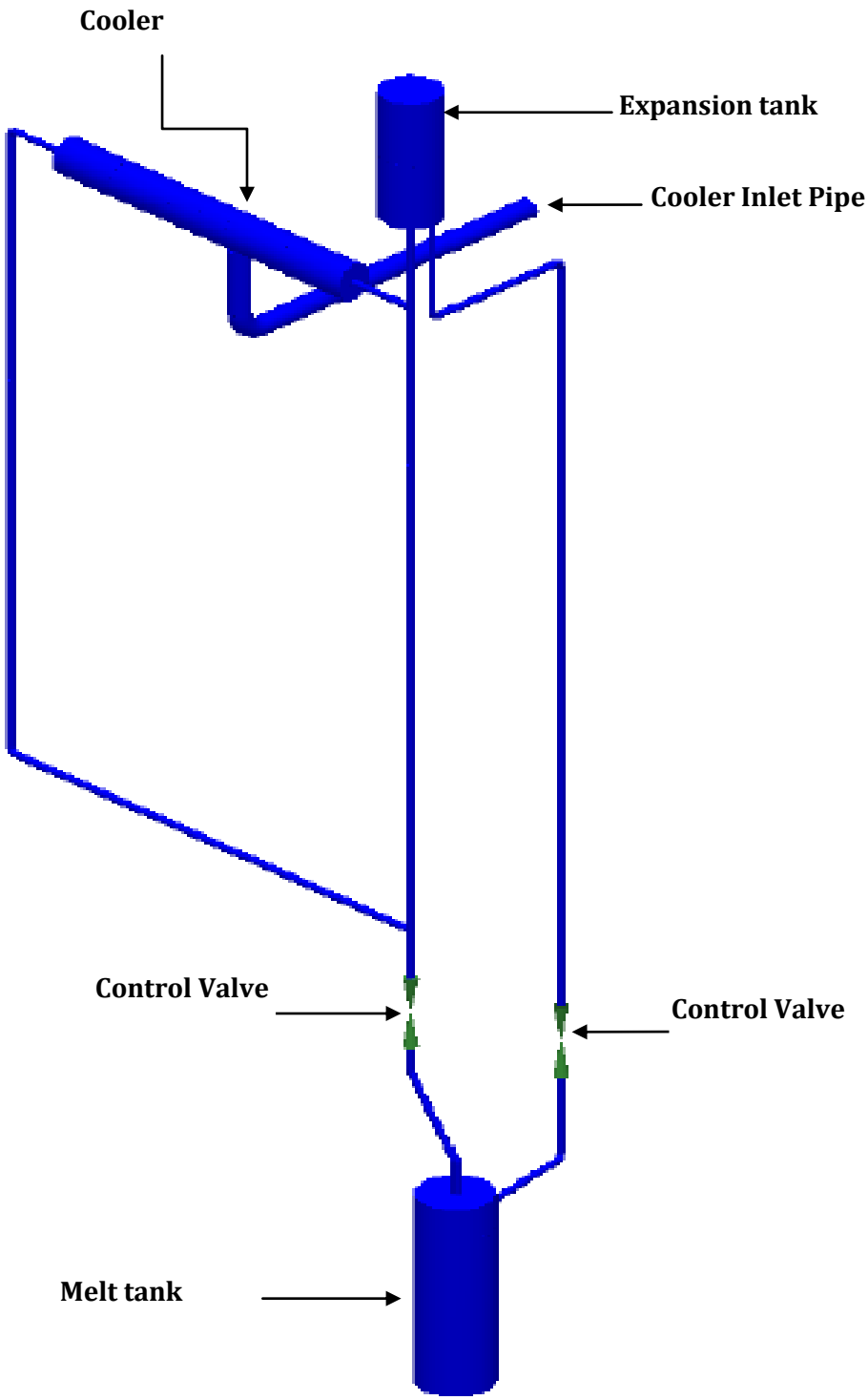

Figure 5. CAESER II Model of MSNCL

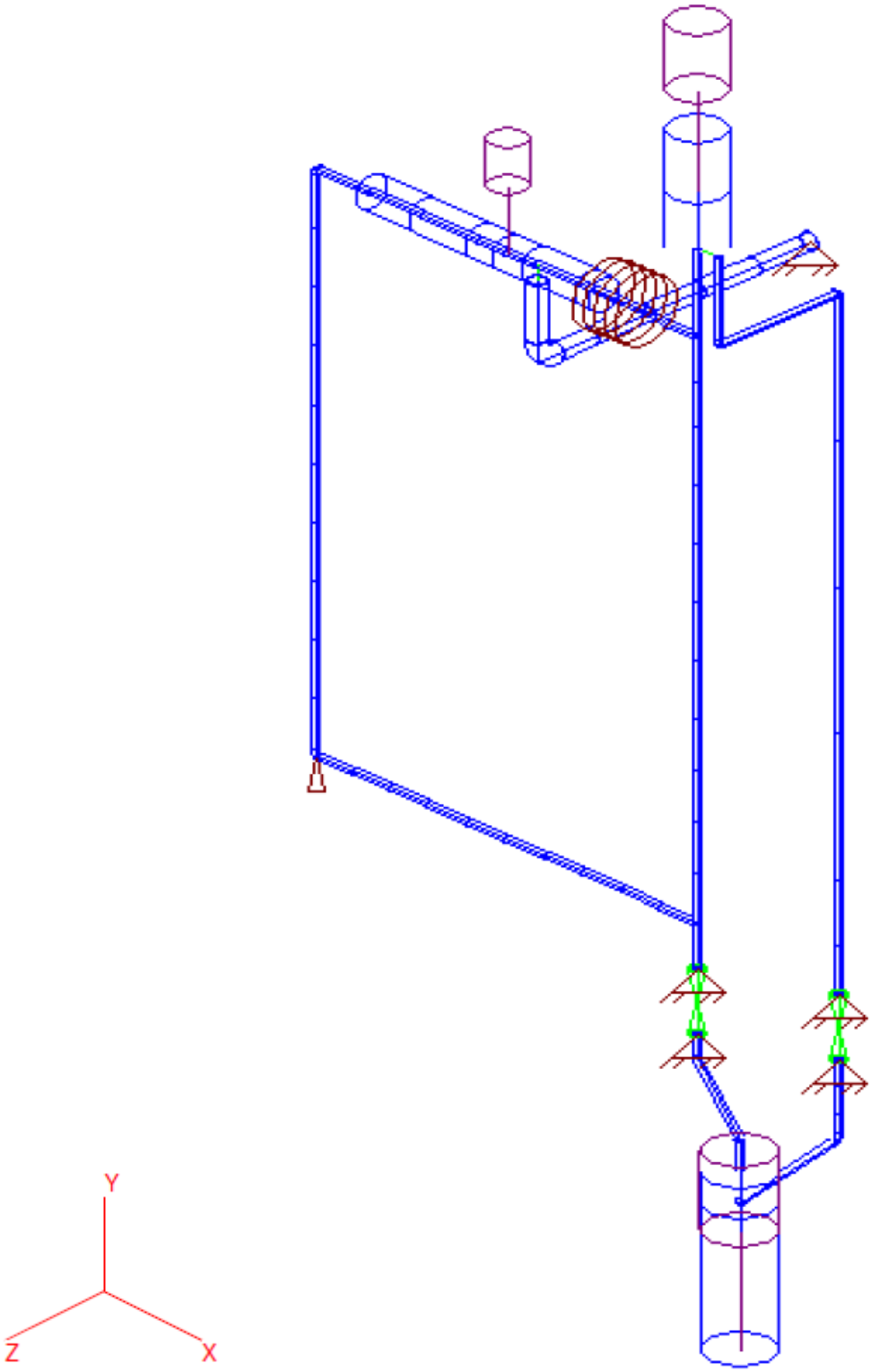

Figure 6 Support scheme for MSNCL

Table 6 Comparison of stresses calculated by CAESER II and piping code ASME B 31.3

Loading case	Maximum Stress calculated by CAESER II (MPa)	Allowable stress given by ASME B 31.3 (MPa)
Sustained Load	77.669 (53.64% of codal stress)	144.788
Expansion Load	266.865 (78.82% of codal stress)	338.577

The support scheme was arrived at after several iterations. In the final scheme, the two control valves have been given a fixed support (anchored). The expansion tank, melt tank and the cooler have been given a spring support and one end of the bottom horizontal leg was simply supported. It has been found that the available supports were suitable enough to accommodate the operating loads.

4.7 Hydro Test of the loop

Hydro test pressure of MSNCL was calculated as per SS 316 material.

The allowable stress (S) of SS 316 as per ASME Section II at room temperature is given as: 1378 kgf/cm^2

The allowable stress (S) of SS 316 as per ASME Section II at 600^oC temperature is given as: 675 kgf/cm^2

Hydro test Pressure (HP) = 1.3 X Design Pressure X (S@30^oC / S@600^oC) (8)

Where S = Allowable stress of SS 316

(S@30^oC / S@600^oC) = Temperature correction factor

Therefore, Hydro Test Pressure = 1.3*5*(20/9.8) = 13.26 kgf/cm^2 ~ 14 kgf/cm^2

4.8 Description of instrumentation and control

The instrumentation and control of the process plays the most important role as the mixture of sodium nitrate and potassium nitrate freezes at around 221°C. Piping and vessel used in the loop are provided with electrically heated surface and band heaters for keeping the nitrate mixture in

molten condition. Surface temperatures on piping and vessels have been monitored and power supply to the heaters has been controlled continuously.

Pressure and level measurements have been done by remote seal type electronic transmitters. Diaphragm of these transmitters was rated up to 300 °C. These instruments sense cover gas pressure and purging gas (argon) pressure and do not face high temperature. Beside this, level of molten nitrates salt has been sensed by discrete type and continuous level probe.

Control valves of ¼" size has been used for controlling cover gas pressure remotely. One isolation valve of size ½" with jacket heater has been used to isolate the melt tank from the loop and another same type of isolation valve has been installed on the over flow line connecting expansion tank and melt tank. These valves are ON/OFF type and electrically controlled.

4.8.1 Type of Instrumentation

The instrumentation provided for this facility has three major objectives. These are data acquisition during experiments, monitoring and control of various parameters for operational requirements and process safety requirements. Two simultaneous failure criteria have not been considered for the design of instrumentation system. All the process parameters have been transmitted electronically to the control room.

Central control system has been located in the control room for processing all the electronic signals transmitted from the field transmitters. The control system digitizes the analog signals, computes the control signals and sends out to the control devices. The supervisory computer serves as operator interface and database server.

All the instruments used are of electronic in nature with 1500VA galvanic isolation. Temperature signals, normalized in the form of 4 to 20 mA DC, are brought to control room using multi-core extension cables. Pressure and differential pressure signals from field are of 4 to 20 mA DC from transmitters energized by 24 VDC power supply located inside the control panel in the control room. 24 VDC ON/OFF signals are brought to control room and sent to field through multi-core cables.

4.8.1.1 Pressure Measurement

Pressure of cover gas (Argon) in melt tank and expansion tank has been measured by SMAR Make remote seal diaphragm based electronic smart transmitters. These transmitters are mounted on second floor on transmitter rack along with the flanges. Gas pressure has been sensed through impulse tubing by the diaphragm, mounted on the flange (Fig. 7). The sensor diaphragm does not face high temperature of the cover gas though it can sense pressure upto a maximum temperature of 300°C.

4.8.1.2 Level Measurement

Levels in the tanks have been measured by measuring differential pressure between cover gas and the liquid at the bottom of the tanks. The pressure of the liquid at the bottom of the tank was sensed by slow purging of argon gas at a constant rate achieved by purge rotameter. This differential pressure has been measured by SMAR Make remote seal diaphragm based electronic smart differential pressure transmitters.

Levels in the tanks were also sensed by conductivity sensors developed in-house. Unlike liquid metals, molten salts have low electrical conductivity and dissociation issues with DC voltage. Experiments were conducted in laboratory to find the suitability of DC voltage for the application of level measurement based on electrical conductivity of molten nitrate salt. It was found that the molten salt gets dissociated at 1 VDC and hence concluded that DC voltage based techniques are not suitable for level detection. A low voltage AC circuit with variable output was designed and assembled. Experiments were conducted again to check the performance of conductivity based level measurement probe for molten salt fluid. It was observed that the molten salt was stable even at 0.7 VAC. This level of AC voltage was sufficient to detect the conducting path of molten salt for level detection application.

Based on conductivity experiments, low voltage AC based level indicating switches having 6 nos. of independent channels was developed, fabricated and installed for high temperature molten salt level indication in the control room. The measurement system generates 0.7 VAC (rms) and injects this AC to molten salt for testing the conductivity. Once the conducting path is confirmed, it switches a DC SSR and there by turning on a 24 DC relay. DC relay sends the signal to control room for indication using LED. These ON/OFF actions of LED is recorded and displayed by SCADA system.

A typical pressure, continuous level measurement and argon filling scheme is given in Fig.7. Figure 8 shows the probe position for discrete measurement of level and temperature in Melt Tank (MT) and Expansion Tank (ET) both.

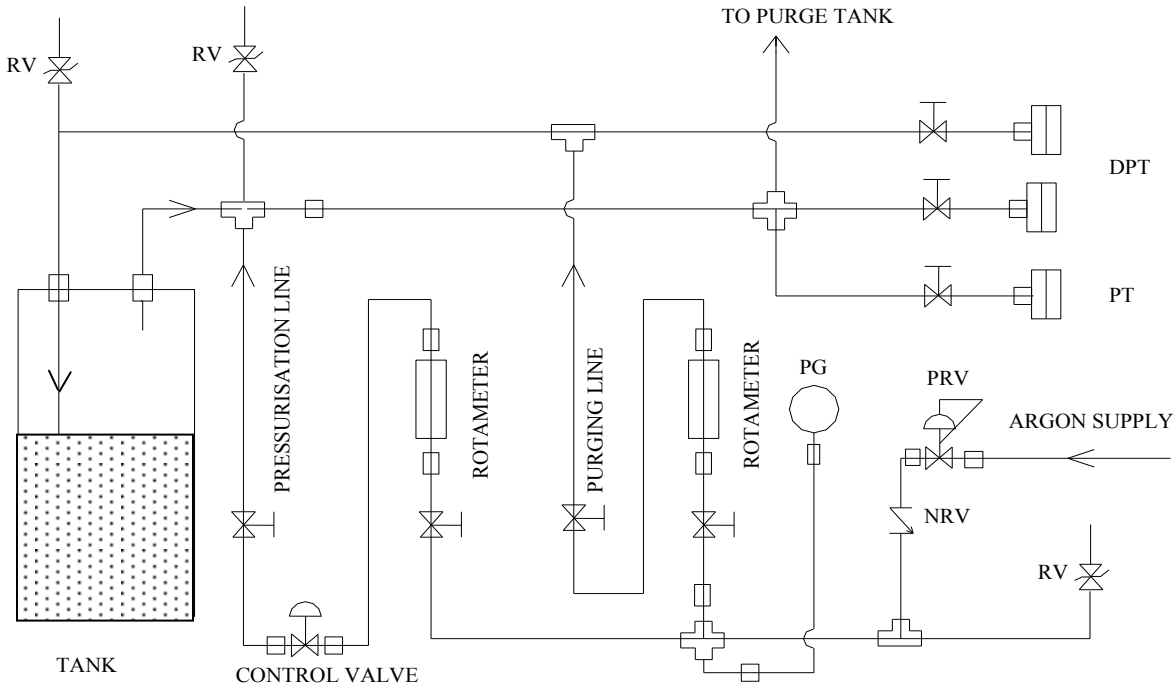

Figure 7. Tubing layout for argon gas supply to pressure transmitters

4.8.1.3 Temperature Measurement

All the temperatures in the loop have been measured by mineral insulated, 1 mm, SS316 and Inconel 625 sheathed; K-Type thermocouples along with ASTRON make isolated electronic temperature transmitters giving 4 to 20 mA normalised floating signals. The transmitters have been calibrated in groups depending on temperature zone in the process.

Locations of thermocouple are on the surface of the pipes and vessels in most of the cases. However, some thermocouples have been inserted in the pipe to sense actual temperature of the fluid using 1 mm Inconel 625 thermocouple fittings. Temperatures of three points inside the tanks have also been measured and the detail scheme is shown in Fig.9.

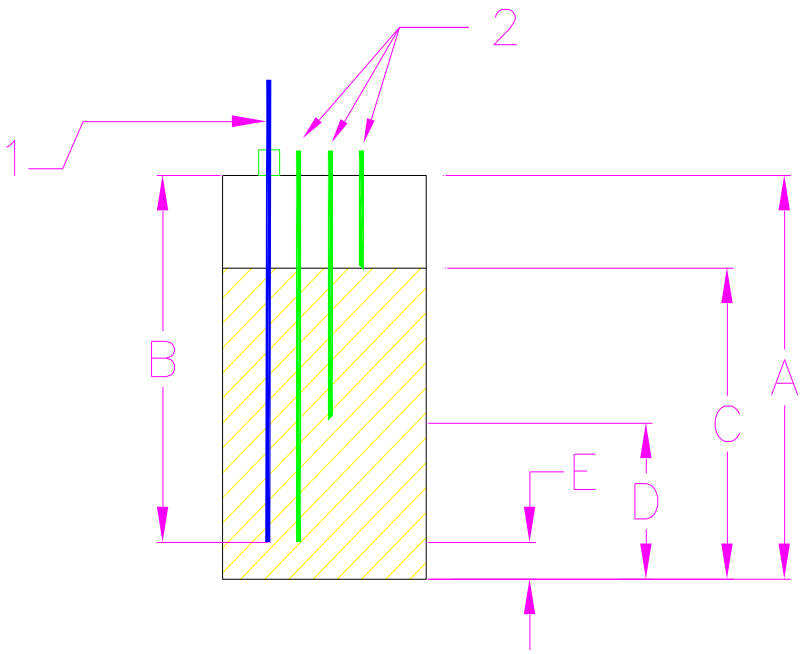

	A	B	C	D	E
MT	520	480	250	150	50
ET	360	340	175	125	25
1 :	THERMOCOUPLE TUBE				
2 :	LEVEL PROBES				

MT: Melt Tank
ET: Expansion Tank

Figure 8. Discrete level measurement probes installed on the tanks

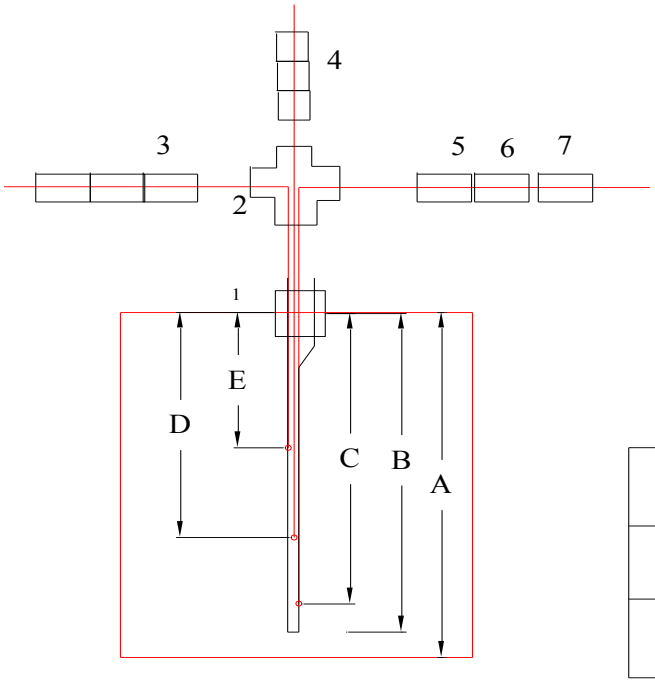

T/C tubing detail for TANKS

1: 1/2" NPT(M)/3/8"TUBE
2: 3/8" TUBE CROSS
3,4,5: 3/8" TUBE/1/4"NPT(F)
6: 1/4"NPT(M)/1/16"NPT(F)
7: 1/16"NPT(M) TC FITTING
EACH BRANCH HAS SAME TYPE OF FITTINGS

	A	B	C	D	E
MT	520	480	470	370	270
ET	360	340	330	240	140

ALL DIMENSIONS ARE IN MM

Figure 9. Tubing layout for three-point temperature measurement at different

4.8.1.4 CONTROL VALVES, PRVs and RVs

Control valves used in this loop are of SS316 with bellow seal. The size of the valves installed on molten salt line is ½" and they have been rated for 500°C and ANSI 900 class where as ¼" size, 400 °C and ANSI 600 class valves has been used on gas (argon) pressure line. The valves on molten salt lines are jacketed with 230 VAC electrical heaters controlled by built-in bi-metallic sensors/solid state power controllers. Thermocouple sensors are also brazed on the surface of the valves and these signals are transmitted to control system for continuous monitoring and controlling the surface temperature of the valves.

4.8.2 Control signal flow (Trips and Alarms)

Signals causing common cause have been grouped together and routed to ensure safe action and hardwire alarms in the appropriate windows. Individual cause for trips and alarm can be seen in detail on the alarm monitor.

Process parameters responsible for operation and safety of the loop are surface temperatures of piping and vessels, molten Salt temperatures at various important points, level in the tanks and cover gas pressure in the tanks. Relief valves have been provided on each tank to take care of accidental pressurization. The signal flow scheme is shown in Fig.10.

4.8.3 Control System

Control System for molten salt loop consists of two major parts. These are field instrumentation and panel instrumentation. Field instrumentation consists of thermocouple temperature sensors with transmitters, pressure and differential transmitters, level switches and level sensors. Panel instrumentation consists of electromechanical relays, solid-state power controllers (SSR), signal conditioners, multi-channel annunciator with push buttons, push button with indicators, independent single digital controllers and high end industrial computer with SCADA software as MMI of the entire system.

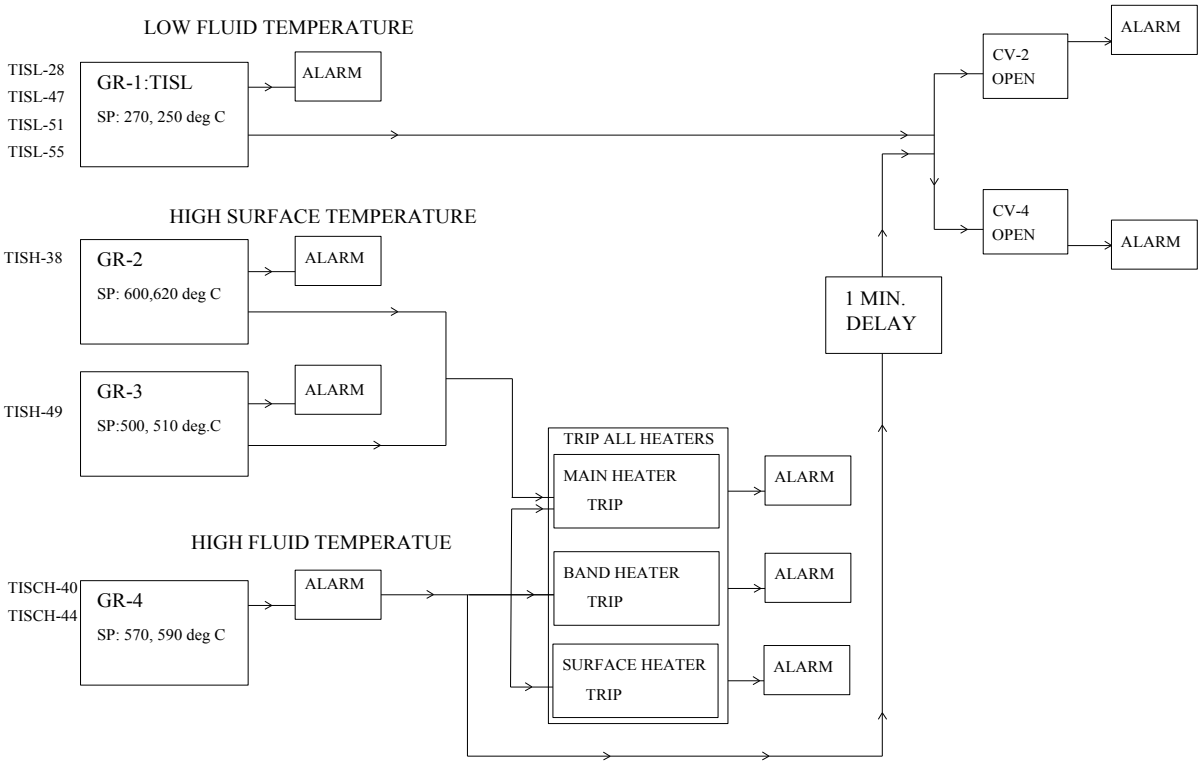

Figure 10. Control signal flow scheme

4.8.4 Hardwire-Controller

Panel mounted single channel hardwired controllers have been used for controlling power supplies to heaters. These controllers have isolated 4 to 20 mA input and time proportional DC output suitable as control signal for SSR. Controllers also have potential free contact outputs which are used for window annunciator and conventional 24 VDC hardwired trip logic for heater trip, valve ON/OFF control and trip annunciation.

4.8.5 SCADA Hardware for Data Acquisition System (DAS)

One industrial PC with quad core processor located in the control panel has been used as supervisory computer and data base server for the loop. All data of the plant are logged and processed by this centralized high performance industrial PC (DAS). It has got 96 nos. of 4-20 mA analog inputs, 2 nos. of isolated analog outputs, 16 nos. of relay outputs. The SCADA acquires and processes data on real time basis and saves in its own internal data base system once in 1 second.

4.8.6 SCADA (MMI) Software

Elipse SCADA application software is serving as front-end operating software of the plant. This application software facilitates as operator interface for process visualization with on-line data on mimic and curve trending with screen update rate up to 1 sample/second for all the selected parameters. It helps operator to prepare reports for desired parameters and formats in excel file.

4.8.7 Electrical Power Control Scheme

There are 12 nos. of surface heaters of rating 500 watts at 230 VAC each, 2 nos. of 2 kW and one 0.5 kW at 230 VAC band heaters. Beside this, there are two surface heaters wrapped on the control valves.

The surface heaters have been mounted on the pipes and valves to maintain the temperature above melting point of the salt. Two larger band heaters mentioned above have been mounted on the surface of melt tank and smaller band heater has been mounted on the surface of expansion tank. A main heater of capacity 2.5 kW has been used for experiment. The main heater was indirect type, electrically heated ½" vertical or horizontal pipe section which can be optionally selected depending on the orientation of heater.

K-type thermocouples have been mounted on surface of this heater (four sections) for protecting it from excessive heating causing damage and also for experimental interests. Each heater power was regulated through a single channel PID controller with time proportional DC pulse output and this was fed to input of a single solid-state ON/OFF type AC power controller. PID controllers work with temperature feedback. There was no temperature feedback control action for main heater control as experiments ware conducted with power as a parameter but heater trip will be actuated at set points.

4.9 Safety of the Loop: Hardware Trips and Relief Valves

4.9.1 Hardwire-Trips

The loop operation has been controlled by independent single channel digital controllers. These controllers accept 4 to 20 mA process parameter inputs and give time proportional DC pulse outputs which has been used as input for solid state relay (SSR) power controllers for controlling the temperature of various sections. Beside this, these digital controllers also have two potential free contact outputs for alarm and trip. Using these trip contacts, hardwired trip circuits have been implemented as per the control signal flow diagram Fig. 10.

Beside this, push buttons with indications have been provided on control panel for switching on and off the loop power supply for all the heaters, power supply of main heater and power supply of auxiliary heaters (all band heaters and surface heaters). Any hardwire trips for the heaters will also cause opening of control valves for collecting the loop inventory in the melt tank.

4.9.2 Relief Valves

Redundant relief valves have been provided on the top of each tank for relieving of excess cover gas pressure. Their discharges have been collected in a common header, which is connected to the exhaust of loop ventilation system. Fire load for MSNCL cabin has also been calculated and detail calculation is given in Annexure-2.

4.10 Instrumentation Power Supply Scheme

The power supply for the instrumentation and control consisted of the following.

1. UPS system
2. 230 V AC, 50 cps, 1 Phase
3. 24 V DC, 5 amps power supply, derived from 230 V AC

4.10.1 Un-interrupted Power Supply System (UPS)

Power supply for instrumentation and control has been provided from an Un-interrupted Power Supply System (UPS) installed in control room. Electrical line supply to UPS has been provided from control panel. The UPS has the following brief specifications.

Input: 230 VAC (nominal), 50 Hz ±5 Hz, 160 to 280VAC Range

Output: 1400 Watts / 2000 VA, 230 VAC Sine wave, 90% efficiency, less than 3% distortion, 50 Hz ±0.1, Hz, 3.1 Crest factor

Battery: for 1-hour minimum operation at full load

4.10.2 230V AC 50 Hz Power Supply

This power supply has been derived from 230 VAC output terminals of UPS and fed to control panel via 6 number of 6A miniature circuit breakers (MCBs) to 24 VDC power supplies (DCPS1 & DCPS2), supervisory computer system. Another 16 point 230 AC distribution box with 32A

MCB has been used to supply the power to small loads (PC, Annunciator, Hooter, Tube light and Fan).

4.10.3 24V, 5A Power Supply

Power Supply to Transmitters and 24V DC Digital Output for SSRs

A power supply distribution box (DCDB) has been installed inside the control panel. A 24 V DC, 5 amps power supply (DCPS1) , derived from 230 V AC, 50 cps, 1 phase, has been wired through the switches s1 to s16 to provide the power supply to the transmitters. Another 24 VDC, 5 amps power supply (DCPS2), derived from 230 V AC, 50 cps, 1 phase, has been looped on control panel TBs to provide the power supply to OEM make electro-mechanical relays, installed on DIN rail in electrical control panel.

4.11 Pneumatic Supply (Air and Argon)

Pneumatic supply available from compressor (7 kgf/cm²) has been provided though PRV attached to each of the control valves for their operation. Argon gas has been used as cover gas for all the tanks and it has also been used to sense the backpressure for level measurement.

In case of compressed air supply failure, or station blackout i.e. total electrical failure of instrumentation power supply, instrument isolation valves can be opened manually for providing supply to control valves for dumping molten salt to melt tank bypassing all engineered control logic. Compressor tank at hall-7 has capacity to supply the compressed air supply for 30 minutes approximately after the failure of compressor. This 30 minutes time was adequate for taking the manual action.

5. THEORETICAL STUDIES FOR NATURAL CIRCULATION FLOWS

Theoretical studies have been performed using in-house developed code LeBENC, an acronym of **Le**ad **B**ismuth **E**utectic **N**atural **C**irculation code. LeBENC is a finite difference, one dimensional code, written to study the steady state and transient behavior of Liquid metal natural circulation loop. A code named TRANCO was available to study the steady state and stability (transient) behavior of natural circulation rectangular loops of uniform diameter for various orientations of heater and cooler. This code has been modified to predict the behavior of liquid metal loop under natural circulation. The major modifications include extension of code applicability to,

1. Non-uniform diameter loops,
2. Different working fluid in primary and secondary side of the loop,
3. General loop geometry
4. Trace heating.

Further this code has been modified to incorporate the thermophysical properties of various molten salt such that, the natural circulation behavior of molten salt could be analyzed. The mathematical formulation and solution procedure used in the LeBENC code and the modification done with respect to molten salt have been discussed in subsequent sections.

5.1 Governing equations

The code is based on basic conservation equation of mass, momentum and energy. In writing energy equation for the wall, the fluid axial conduction is considered as it might play important role in molten salt loop.

5.1.1 Energy equation for fluid

$$\frac{\partial T}{\partial t} - \alpha \frac{\partial^2 T}{\partial s^2} + \frac{W}{A_{in}\rho_0}\left(\frac{\partial T}{\partial s}\right) = \frac{-4h_{in}(T - T_w)}{\rho_0 D_{in}\ Cp} \tag{9}$$

In Eq. 9 'h_{in}' is the heat transfer coefficient between wall and primary fluid and subscripts '*in*' and '*w*' are used for 'inside' and 'wall'. It is to be noted that the right hand side of the equation is applicable to the heat source as well as heat sink and the connected pipes.

5.1.2 Momentum equation for fluid

Assuming Boussinesq approximation to be valid, the momentum equation, for 1-D incompressible flow neglecting viscous dissipation, for 'i^{th}' node can be written as,

$$\begin{aligned} &\frac{\Delta s_i}{A_{in}}\frac{dW}{dt} = \rho_0 g(1 - \beta(T_i - T_0))\Delta z_i \\ &-\frac{f_i \Delta s_i}{D_{in.i}}\left(\frac{W}{2\rho_0 A_{in,i}^{\ 2}}\right) - k_i\left(\frac{W^2}{2\rho_0 A_{in,i}^{\ 2}}\right) - \Delta p_i - \Delta p_{acc,i} \end{aligned} \tag{10}$$

where, f_i is friction factor expressed by the following equation.

$$f_i = p\ Re_i^{-b} \tag{11}$$

The constants '*p*' and '*b*' depends upon the nature of flow (for laminar flow *p=64* and *b=1* and for turbulent flow *p=0.316* and *b=0.25*). The subscript '*i*' denotes any 'i^{th}' node of the loop. In

buoyancy term, the density is given by the following equation which is valid over small temperature ranges

$$\rho = \rho_0 \left[1 - \beta(T - T_0)\right] \tag{12}$$

Now, the summation of acceleration pressure drop and static pressure drop in a closed loop becomes zero. Therefore, the above equation can be written as,

$$\sum_{i=1}^{N} \frac{\Delta s_i}{A_{in,i}} \frac{dW}{dt} = \rho_0 g \beta \sum_{i=1}^{N} T_i \Delta z_i - \sum_{i=1}^{N} \frac{f_i \Delta s_i}{D_{in,i}} \left(\frac{W}{2\rho_0 A_{in,i}^2} \right) - \sum_{i=1}^{N} k_i \left(\frac{W^2}{2\rho_0 A_{in,i}^2} \right) \tag{13}$$

5.1.3 Conduction equation for the wall

Heat loss from the pipe wall is considered in writing conduction equation for the pipe wall.

$$\frac{\partial T_w}{\partial t} - \alpha_w \frac{\partial^2 T_w}{\partial S^2} = -\frac{4h_{in}(T_w - T)}{\rho_w C p_w} \left(\frac{D_{in}}{(D_o^2 - D_{in}^2)} \right) - \frac{4h_o(T_w - T_x)}{\rho_w C p_w} + \frac{4q}{\rho_w C p_w} \left(\frac{D_o}{(D_o^2 - D_{in}^2)} \right) \tag{14}$$

Where,

for pipes $T_x = T_a$, $h_o = h_a$ *and* $q = 0$

for cooler $T_x = T_s$, $h_o = h_s$ *and* $q = 0$

for heater $h_o = 0$ *and q specified*

5.2 Discretization scheme

Out of several possible ways to discretize the governing equations, the explicit method for discretizing energy equation for fluid and the implicit method for discretizing the momentum equation is used.

5.2.1 Discretization of energy equation for fluid

First order explicit upwind scheme and central difference scheme is used to discretize the convective term and the diffusion term respectively. The discretized energy balance equation for 'i^{th}' node of the fluid can be written as follows,

$$\left(\frac{T_i^{n+1}-T_i^n}{\Delta t}\right)= \alpha\left(\frac{T_{i+1}^n-2T_i^n+T_{i-1}^n}{\Delta s_i^{\,2}}\right) \\ -\frac{W}{\rho_0 A_{in,i}}\left(\frac{T_i^n-T_{i-1}^n}{\Delta s_i}\right)-\frac{4h_{in,i}}{D_{in,i}\rho_0 Cp}(T_i^n-T_{w,i}^{n+1}) \tag{15}$$

After some algebraic manipulations, the above equation can be written as,

$$T_i^{n+1}=a_{i+1}^n T_{i+1}^n+a_i^n T_i^n+a_{i-1}^n T_{i-1}^n+b_i^{n+1} \tag{16}$$

For $W>0$ the values of coefficients in Eq. 16 are given by,

$$\left.\begin{aligned} a_{i+1}^n &= Fo_i^n \\ a_i^n &= \left(1-2Fo_i^n-Co_i^n-\frac{4h_{in,i}\Delta t}{\rho_0 CpD_{in,i}}\right) \\ a_{i-1}^n &= Fo_i^n+Co_i^n \\ b_i^n &= \frac{4h_{in,i}\Delta t T_{w,i+1}^{n+1}}{\rho_0 CpD_{in,i}} \end{aligned}\right\} \tag{17}$$

where, Fo_i^n and Co_i^n are Fourier number and Courant number respectively calculated at n^{th} time level and are given by,

$$Fo_i^n=\frac{\alpha\ \Delta t}{\Delta s_i^{\,2}}\ ,\ Co_i^n=\left(\frac{W^n\Delta t}{\rho_0 A_{in,i}\Delta s_i}\right)\Bigg\} \tag{18}$$

For $W<0$ the values of coefficients in Eq. 16 are given by,

$$\left.\begin{aligned} a_{i+1}^n &= Fo_i^n-Co_i^n \\ a_i^n &= \left(1-2Fo_i^n+Co_i^n-\frac{4h_{in,i}\Delta t}{\rho_0 CpD_{in,i}}\right) \\ a_{i-1}^n &= Fo_i^n \\ b_i^n &= \frac{4h_{in,i}\Delta t T_{w,i+1}^{n}}{\rho_0 CpD_{in,i}} \end{aligned}\right\} \tag{19}$$

Again, the coefficients of T_i^{n+1}, T_{i-1}^n and T_{i+1}^n are all positive but that of T_i^n may be negative. Therefore the limiting time step to keep the coefficient positive is expressed as

for $W>0$

$$\Delta t = \frac{1}{\left(\frac{2\alpha}{\Delta s_i^{\,2}} + \frac{W^n}{\rho_0 A_{in,i} \Delta s_i} + \frac{4h_{in,i}}{\rho_0 CpD_{in,i}} \right)} \tag{20}$$

for W<0

$$\Delta t = \frac{1}{\left(\frac{2\alpha}{\Delta s_i^{\,2}} - \frac{W^n}{\rho_0 A_{in,i} \Delta s_i} + \frac{4h_{in,i}}{\rho_0 CpD_{in,i}} \right)} \tag{21}$$

It has to be noted that time step is function of mass flow rate. Therefore, time step has to be recalculated for each new time level.

5.2.2 Discretization of Momentum equation

Now, while solving momentum equation T_i^{n+1} is available. Therefore implicit scheme for discretizing momentum equation is used as shown in Eq. 22 below.

$$\begin{aligned} &\sum_{i=1}^{N} \frac{\Delta s_i}{A_{in,i}} \frac{W^{n+1} - W^n}{\Delta t} = \rho_0 g \beta \sum_{i=1}^{N} T_i^{n+1} \Delta z_i \\ &- \sum_{i=1}^{N} \left(\frac{f_i \Delta s_i}{D_{in,i}} + k_i \right) \left(\frac{W^{n+1^2}}{2\rho_0 A_{in,i}^{\,2}} \right) \end{aligned} \tag{22}$$

Above equation, after some algebraic manipulation, can be written as,

$$\begin{aligned} W^{n+1} = W_n &- \left(\frac{c_2}{c_1} \Delta t \right) W^{n+1} \left| W^{n+1} \right| \\ &+ \left(\frac{c_3}{c_1} \Delta t \right) \sum_{i=1}^{N} T_i^{n+1} \Delta z_i \end{aligned} \tag{23}$$

where C_1, C_2 and C_3 are given by,

$$\left.\begin{aligned} C_1 &= \sum_{i=1}^{N} \frac{\Delta s_i}{A_{in,i}} \\ C_2 &= \sum_{i=1}^{N} \left(\frac{f_i \Delta s_i}{D_{in}} + k_i \right) \left(\frac{1}{2\rho_0 A_{in}^{\ 2}} \right) \\ C_3 &= \rho_0 g \beta \end{aligned} \right\} \tag{24}$$

5.2.3 Discretization of Conduction equation for the wall

Discretized energy balance equation for 'i^{th}' node of wall can be written as

$$\begin{aligned} &\left(\frac{T_{w,i}^{n+1} - T_{w,i}^{n}}{\Delta t} \right) = \alpha_w \frac{(T_{w,i+1}^{n} - 2T_{w,i}^{n} + T_{w,i-1}^{n})}{\Delta s_i^{\ 2}} \\ &- \frac{4h_{in,i}(T_{w,i}^{n} - T_i^{n})}{\rho_w C p_w} \left(\frac{D_{in,i}}{D_{o,i}^2 - D_{in,i}^2} \right) \\ &- \frac{4h_o(T_{w,i}^{n} - T_x^{n})}{\rho_w C p_w} \left(\frac{D_{in,i}}{D_{o,i}^2 - D_{in,i}^2} \right) + \frac{4q''}{\rho_w C p_w} \left(\frac{D_{o,i}}{D_{o,i}^2 - D_{in,i}^2} \right) \end{aligned} \tag{25}$$

After some algebraic manipulation above equation can be written as

$$T_{w,i}^{n+1} = a_{w,i+1}^{n} T_{w,i+1}^{n} + a_{w,i}^{n} T_{w,i}^{n} + a_{w,i-1}^{n} T_{w,i-1}^{n} + b_{w,i}^{n} \tag{26}$$

Where,

$$\left.\begin{aligned} a_{w,i+1}^{n} &= Fo_{w,i}^{n} \\ a_{w,i}^{n} &= \left(\begin{aligned} &1 - 2Fo_{w,i}^{n} - \frac{4h_{in,i}}{\rho_w C p_w} \frac{D_{in,i}}{(D_{o,i}^2 - D_{in,i}^2)} \Delta t \\ &- \frac{4h_o}{\rho_w C p_w} \frac{D_{in,i}}{(D_{o,i}^2 - D_{in,i}^2)} \Delta t \end{aligned} \right) \\ a_{w,i-1}^{n} &= Fo_{w,i}^{n} \\ b_{w,i}^{n} &= \left(\begin{aligned} &\frac{4h_{in,i}}{\rho_w C p_w} \frac{D_{in,i}}{(D_{o,i}^2 - D_{in,i}^2)} T_i^{n} \\ &+ \frac{4h_o}{\rho_w C p_w} \frac{D_{in,i}}{(D_{o,i}^2 - D_{in,i}^2)} T_{x,i}^{n} \\ &+ \frac{4q''}{\rho_w C p_w} \frac{D_{in,i}}{(D_{o,i}^2 - D_{in,i}^2)} \end{aligned} \right) \Delta t \end{aligned} \right\} \tag{27}$$

$Fo_{w,i}^{n}$ is given by

$$Fo_{w,i}^{n} = \frac{\alpha_w \Delta t}{\Delta s_i^{2}} \tag{28}$$

The coefficients of $T_{w,i}^{n+1}, T_{w,i-1}^{n}$ and $T_{w,i+1}^{n}$ are all positive but that of $T_{w,i}^{n}$ may be negative. Therefore the limiting time step to keep the coefficient of positive is expressed as

$$\Delta t = \left(2\frac{\alpha_w}{\Delta s_i^{2}} + \frac{4h_{in,i}}{\rho_w Cp_w}\frac{D_{in,i}}{(D_{o,i}^2 - D_{in,i}^2)} + \frac{4h_o}{\rho_w Cp_w}\frac{D_{in,i}}{(D_{o,i}^2 - D_{in,i}^2)} \right)^{-1} \tag{29}$$

The minimum of the time steps, as calculated by Eq. 20, Eq. 21 and Eq. 29, is taken for calculation in each time level.

5.3 Solution procedure adopted in the code

For convenience in calculation, the length of the node in wall and fluid is taken equal. These nonlinear and coupled equations are then solved iteratively using the procedure mentioned below.

(1) The minimum of the time steps as calculated from Eq. 20 or Eq. 21 and Eq. 29 is taken for calculation.

(2) Discretized wall energy equation i.e., Eq. 26 is solved explicitly using above time step to obtain $T_{w,i}^{n+1}$.

(3) Using $T_{w,i}^{n+1}$ in discretized energy balance equation for fluid i.e., Eq. 16, nodal fluid temperature at new time level (i.e., T_i^{n+1}) is obtained.

(4) Temperature integral $\sum_{i=1}^{N} T_i^{n+1} \Delta z_i$ in momentum balance equation i.e., in Eq. 23, is evaluated by using the Trapezoidal rule or Simpson's rule.

(5) Flow rate at new time level i.e., W^{n+1} is obtained by solving discretized momentum equation i.e., Eq. 23.

Step (1) to (5) is repeated until steady state is achieved.

5.4 Geometry and Nodalization of MSNCL considered in LeBENC

For the sake of analysis the whole loop has been divided into segments. There are total 22 segments in the molten salt loop and each segment has been divided into nodes. The nodal diagram of the loop for VHHC orientation is shown in the Fig. 11. Segment L1 and L7 denote the heater and cooler respectively. L2, L6, L8, L11, L13, L16, L18 and L22 represent the pair of flanges mounted at heater and cooler inlet/outlet positions for all orientations. Dimensions of the segments modeled in LeBENC are listed in Table 7.

5.5 Input for analysis using LeBENC

Temperature dependent thermophysical properties of molten nitrate salt mixture have been used for simulation. These properties are calculated in each time step by incorporating recommended correlations derived in Appendix-1. The properties of piping material, Inconel 625 has been taken from special metals [21]. The local hydraulic loss coefficients in various components and piping's have been calculated from Idelchik et. al. The detail calculation for local loss coefficient has been provided in Appendix-3. It has been seen analytically, the flow in MSNCL was always in laminar regime upto given maximum power of 2500W. Therefore, heat transfer coefficient in the heater and cooler (primary side) were calculated by analytical value $Nu = 4.36$ for constant heat flux condition.

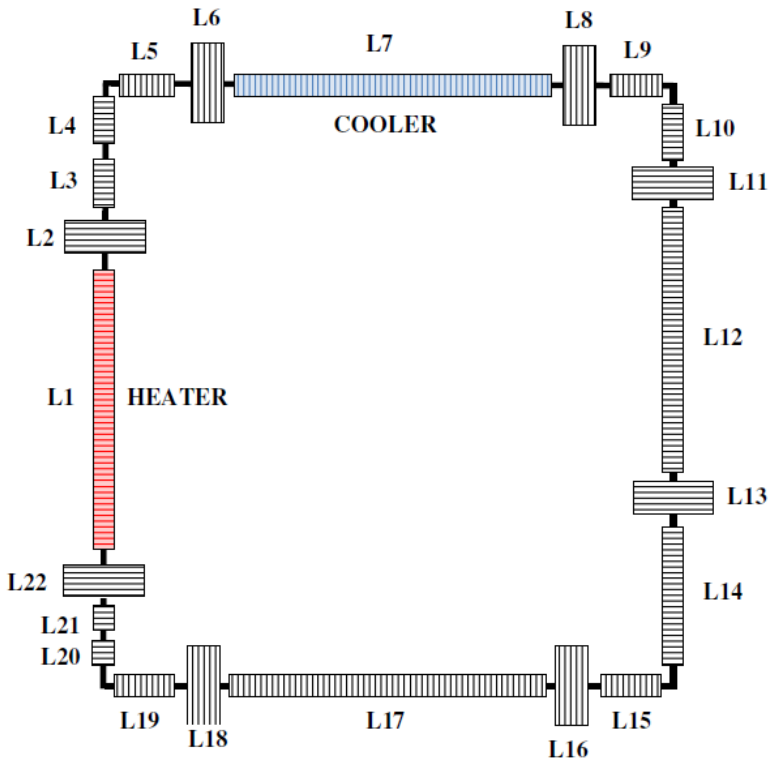

Figure 11. Nodal diagram of MSNCL modeled in LeBENC

6. TEST PROCEDURE AND MATRIX OF THE EXPERIMENTS PERFORMED

Before the steady state and transient experiments, preparatory test was carried out to commission the loop. For filling the salt, the whole loop was heated above 300^{o}C. Molten salt temperature in the melt tank was then increased 350^{o}C. With the help of argon gas pressure the molten salt from the melt tank was pushed to fill the entire loop and finally to expansion tank. An overflow line has been provided from expansion tank to melt tank which prevented the excess filling of molten salt into the loop. After a fixed level of the salt in expansion tank, excess molten salt came back to melt tank through overflow line. The different experiments performed in the loop have been listed in Table 8.

Figure 12 shows the mimic of MSNCL used for online monitoring of various process parameters viz. salt temperature, surface temperature, cover gas pressure, level in the tanks, positions of thermocouples and heaters etc.

Table 7. Dimensions for the segments of MSNCL modeled in LeBENC

Segment	Nodes	Thickness of Pipe (m)	Length (m)	K-factor
L1	15	0.0039	0.960	0.001
L2	5	0.04	0.04	0.001
L3	15	0.0039	0.130	0.001
L4	15	0.0039	0.655	0.68
L5	15	0.0039	0.151	0.001
L6	5	0.150	0.150	0.001
L7	15	0.0039	0.870	0.001
L8	5	0.200	0.150	0.001
L9	15	0.0039	0.179	0.68
L10	15	0.0039	0.180	0.001
L11	5	0.04	0.04	0.001
L12	15	0.0039	1.160	0.001
L13	5	0.04	0.04	0.001
L14	15	0.0039	0.580	0.68
L15	15	0.0039	0.180	0.001
L16	5	0.04	0.04	0.001
L17	15	0.0039	0.960	0.001
L18	5	0.04	0.04	0.001
L19	15	0.0039	0.180	0.68

L20	15	0.0039	0.08	0.001
L21	15	0.0039	0.095	0.001
L22	5	0.04	0.04	0.001

Figure 13 shows the initial heating of the loop, filling of molten salt, establishment of natural circulation and steady state achievement of the loop in form of molten salt temperature at heater and cooler inlet/outlet positions. The graph shows the argon gas temperature inside the loop up to 19300 s, after that molten salt filing was started. During filling, argon gas from the loop was purged and replaced with molten salt. Simultaneously, main heater power is set at 1200W and secondary side air blower was switched on. Subsequently, the temperature of the molten salt increased for the next 1500s and then decreased at all four locations. Finally after 28000s the loop attained steady state. The startup transient of the loop is zoomed out and shown in the same Fig. 13.

Various steady state and transient experiments have been performed in MSNCL. The transients presented in this report are focused on step change in heater power, loss of heat sink and heater trip. These transients are considered important for the safety assessment of molten salt based systems. In addition to these, the operational transients concerned with startup of the loop have also been performed.

Prior to each transient, steady state conditions was established in the loop which were the initial conditions of the transients. The steady state runs also helped to check the performance of the instrumentation before the transient begin. For the integrity and safety of the loop, most transients were mitigated by re-starting the cooler or changing the main heater power for safe operating range of 300^{o}C to 550^{o}C.

All the steady state and transient tests performed have been listed in Table 8. The detailed test procedures have been described in Section-7 of this report together with the experimental results and post-test analysis results obtained using LeBENC code.

7. RESULTS AND DISCUSSIONS

MSNCL has been operated to study the steady state and transient behavior of molten nitrate salt. Steady state correlation given by Vijayan et. al. as well as steady state results obtained using LeBENC have been compared with experimental data. LeBENC.code has also been used for analyzing various transients and results obtained have been compared with experimental data.

7.1 Steady state analysis

In the steady state natural circulation experiment, the loop was allowed to reach steady state conditions at different powers. By observing the trend of molten salt temperature at different location, the steady state conditions were judged.

For steady state natural circulation, Vijayan et. al. [14,18,19] showed that the flow in single phase uniform or non-uniform diameter natural circulation loops can be expressed as,

$$\mathrm{Re}_{ss} = C\left[\frac{Gr_m}{N_G}\right]^r \tag{30}$$

Where, constants 'c' and 'r' depends upon the nature of flow i.e. laminar or turbulent. Parameter N_G depends upon geometry of the loop. The detailed derivation of Eq 30 can be found in Vijayan [18]. Re_{ss} and Gr_m are based on the reference diameter. As per Vijayan, the flow can be considered turbulent if Gr_m >5.0E12. Based on this, in the present study it was seen that for the operating power range i.e. from 1200W to 2000W the flow remain in laminar regime for VHHC orientation.

Selecting the correlation for laminar flow regime, the correlation has been compared with experimental data in Fig 14. It has been found that the experimental results uniformly lag with correlation values due the heat losses in the loop. There was approximately 30% heat loss in the loop which came as an error in the given comparison.

Theoretical analysis for steady state cases has also been carried out for different powers of main heater using LeBENC. Figure 15 shows the comparison of main heater inlet and outlet temperatures at different power calculated by LeBENC code with that of experimental data. The comparison shows that the predicted results of LeBENC are in good agreement with experimental data.

The temperature distribution in entire length of the loop is shown in Fig. 16 and Fig. 17. The comparison of LeBENC code prediction with the experimental values have been plotted in this figure. Figure 16 shows the fluid temperature distribution inside the loop and Fig 17 shows the pipe wall outer surface temperature around the loop. In both the figures steady rise in

temperature could be seen in main heater of the loop and steady drop could be seen in cooler. In the piping there was small temperature drop due to heat losses. These heat losses have been quantified with experimental results and then outside heat transfer coefficient has been calculated for each segment of the loop. The same has been incorporated in LeBENC for its validation. Comparison of LeBENC results with experimental data shows good agreement.

Table 8 Test matrix for experiment in MSNCL

Experiment		**Initial Condition**	**Procedure**
Steady state and step change in power transient.		Molten salt temperature is constant with time with some fixed main heater power, W_s=0.02kg/s	Increase or decrease the power of the main heater and allow the system to come to new steady state.
i.	1st transient	Steady state at 1200W	Main heater power change to 1500W
ii.	2nd transient	Steady state at 1500W	Main heater power change to 1600W
Loss of heat sink		Steady state at 1500W, W_s=0.02kg/s, molten salt temperature at heater outlet = 352°C	Secondary side air flow is stopped by switching of the blower i.e. W_s=0
Heater trip		Steady state at 2000W, W_s=0.02kg/s, molten salt temperature at cooler outlet = 410°C	Main heater power setting is changed to zero.

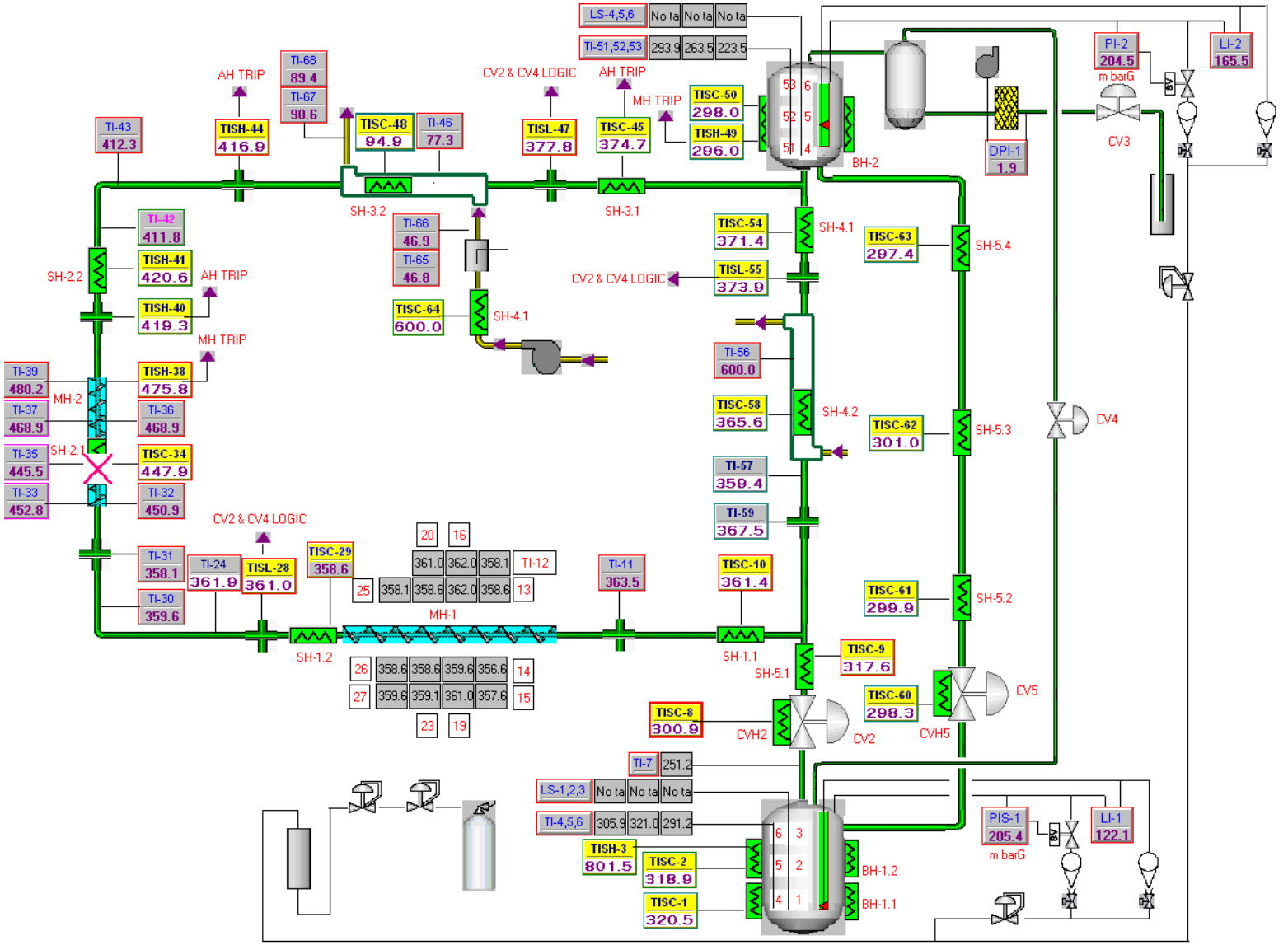

Figure 12. Mimic of MSNCL for showing various online parameters

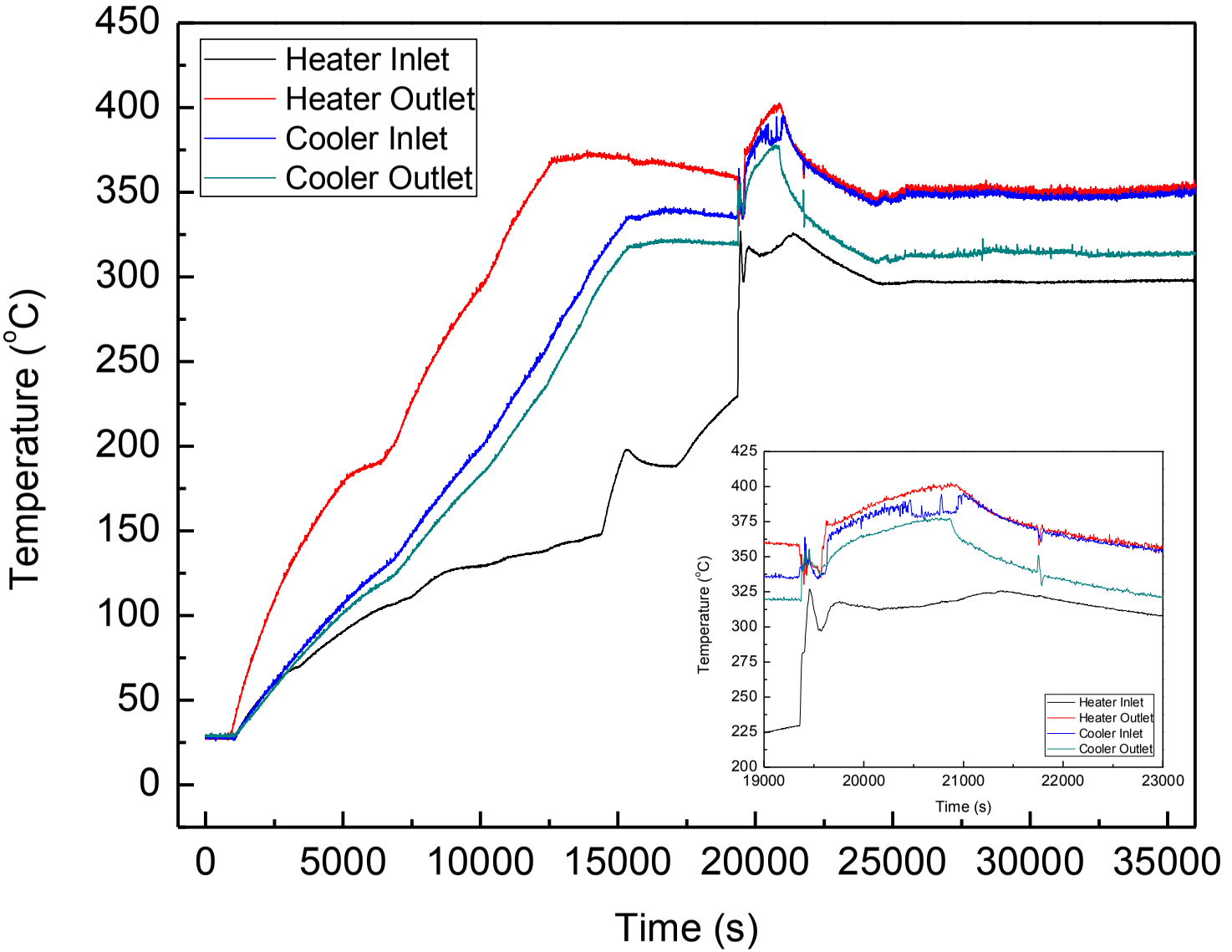

Figure 13. Startup of Natural Circulation at 1200W

7.2 Transient studies

Transient studies were carried out to simulate some postulated accidental scenario in the molten salt based systems. The main objective was to observe the behavior of molten salt during various transient conditions. The transient experimental studies include step power change in the loop, loss of heat sink transient and heater trip transient.

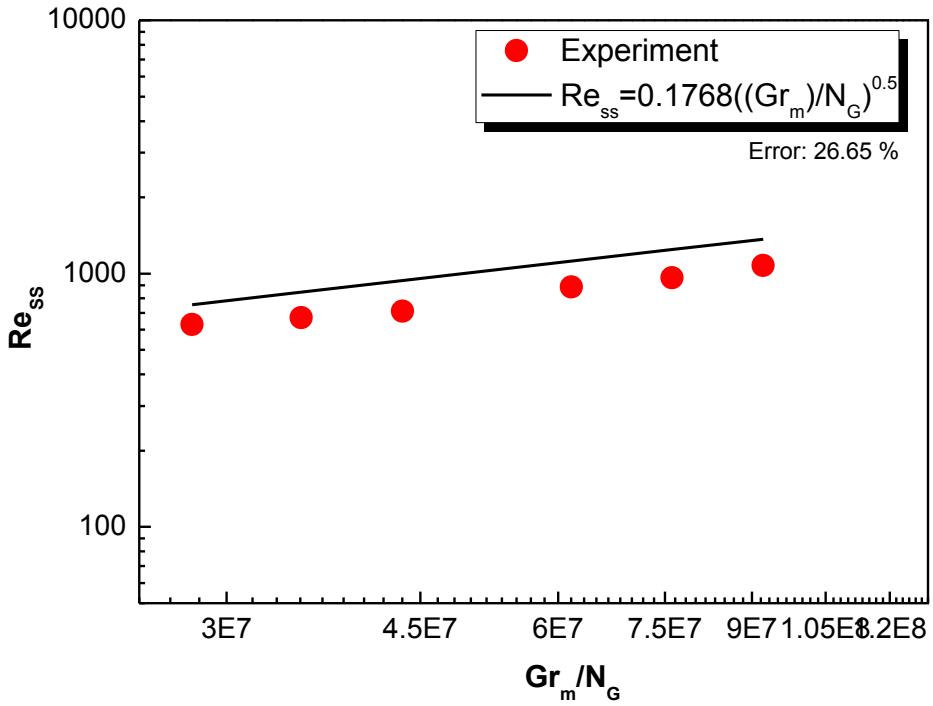

Figure 14. Comparison of experimental Data with steady state correlation given by Vijayan et. al.

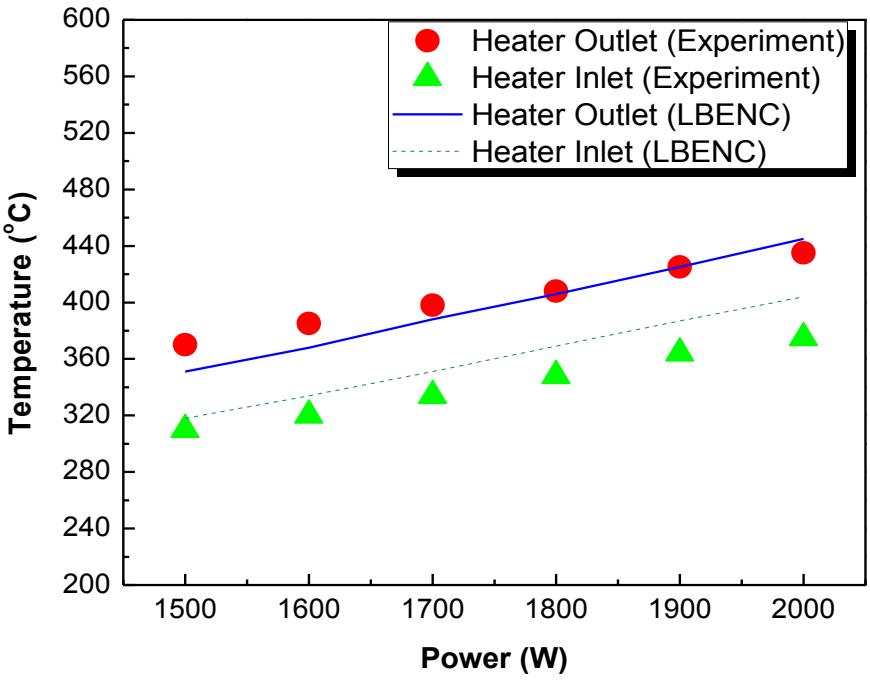

Figure 15. Steady state temperature of molten salt at heater inlet and outlet for different power and its comparison with LeBENC

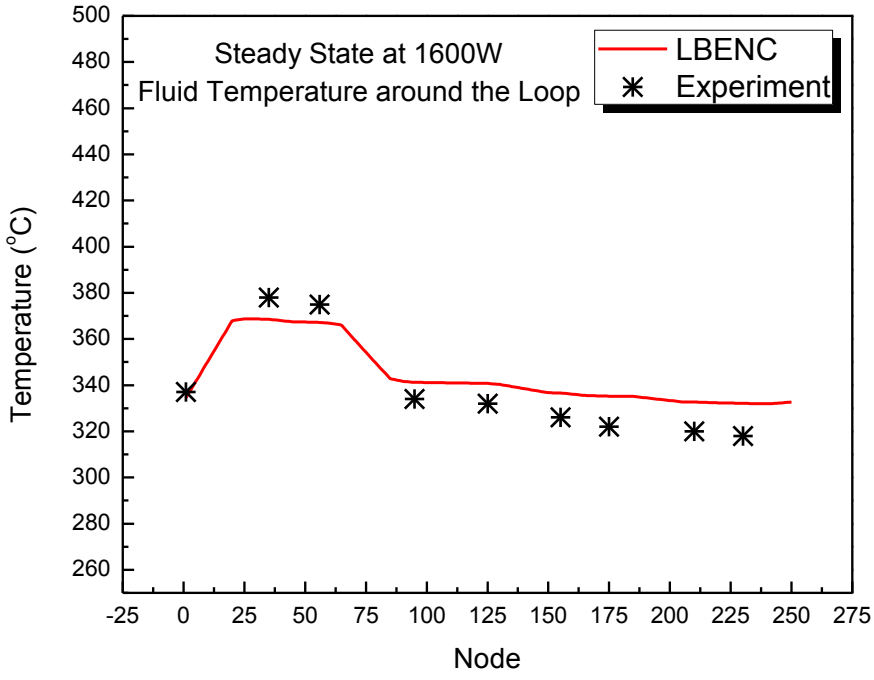

Figure 16. Steady state temperature of fluid around the loop and its comparison with LeBENC

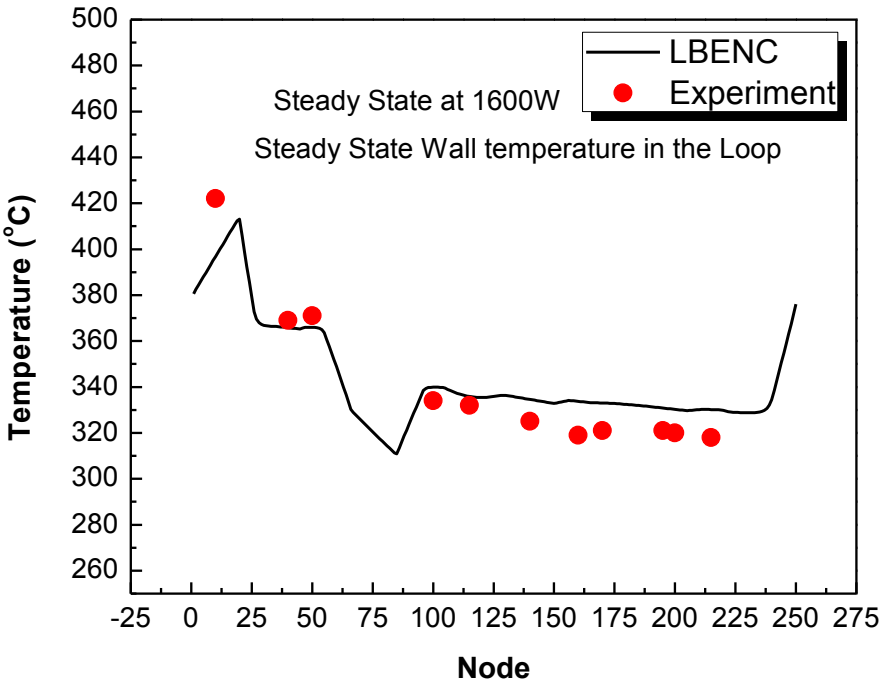

Figure 17. Steady state temperature of fluid around the loop and its comparison with LeBENC

7.2.1 Step Power Change Transient

In solar power tower systems the solar rays are concentrated on the receiver with the help of heliostat. It may possible that some time few rays opted outside the receiver. This may change the input power of the receiver. Considering this into mind a step change in main heater power transient was carried out in MSNCL.

Initial condition for this transient was as follows: The loop was in steady state at 1200W power. The secondary side air flow rate was maintained at 0.02kg/s. The transient was started by increasing the main heater power to 1500W from 1200W by keeping the secondary side air flow rate constant at initial value. The effect of this power change is shown in Fig. 18 in terms of change in temperature. Heater outlet and cooler inlet temperature increases sharply just after increasing the main heater power and finally attained steady state temperature at nearly 2400s. Figure 19 again shows the variation of temperature with change in power from 1500W to 1600W for constant air flow rate in secondary side. It can be seen from Fig. 19 that the steady state reached at higher temperature level with smooth rise. Theoretical analysis for step power change

has been studied. Figure 18 and Fig. 19 shows the variation of heater outlet and cooler inlet temperature predicted using LeBENC and comparison of the same with experimental data.

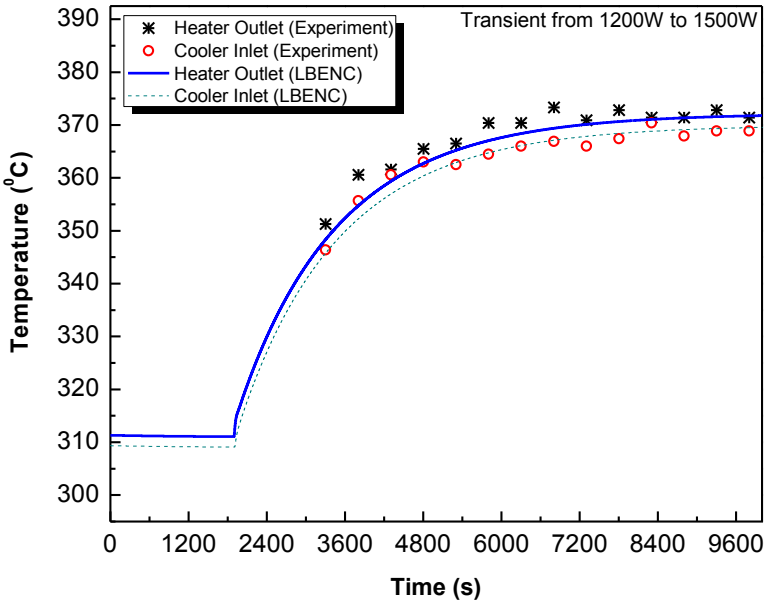

Figure 18. Step power change transient from 1200W to 1500W and its comparison with LeBENC

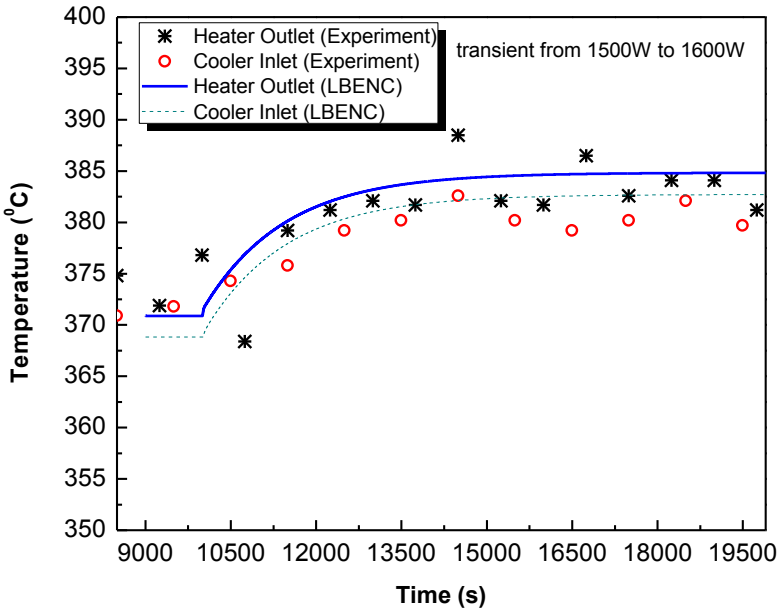

Figure 19. Step power change transient from 1500W to 1600W and its comparison with LeBENC

7.2.2 Loss of Heat Sink (LOHS)

A loss of heat sink event is usually considered in the safety analysis for all types of heat transport systems. Its consequences are often quite severe and most safety analyses have to assure good predictions. Thus the data presented for this type of transient is very important for purpose of code validation.

The initial condition for one of the transients performed is as follows: loop was in steady state at 1500W power; secondary side air flow was maintained with flow rate of 0.02kg/s. The transient was initiated as follows: steady state conditions were established. Then the air blower was switched off and subsequently the secondary flow was completely stopped. In result to that the coolant temperature increased due to the loss of heat sink and to avoid the threat to the integrity of the facility due to overheating, air blower was re-started at fluid temperature of 413^{o}C. This action forced the molten salt to flow back to steady state value and the initial steady state conditions were re-established.

As shown in Fig. 20 at the start of the transient, cooler outlet temperature increased rapidly and came closer to the cooler inlet temperature due to the loss of cooling. This temperature jump was accomplished quickly and the inlet and outlet temperature of the cooler then increased together. A sharp increase in the heater outlet and cooler inlet temperature was also seen in Fig. 21. The main result of the loss of heat sink transient is that the temperature of molten salt and all of the loop structural materials increases with time. Results of LeBENC are compared with experimental data and found in good agreement.

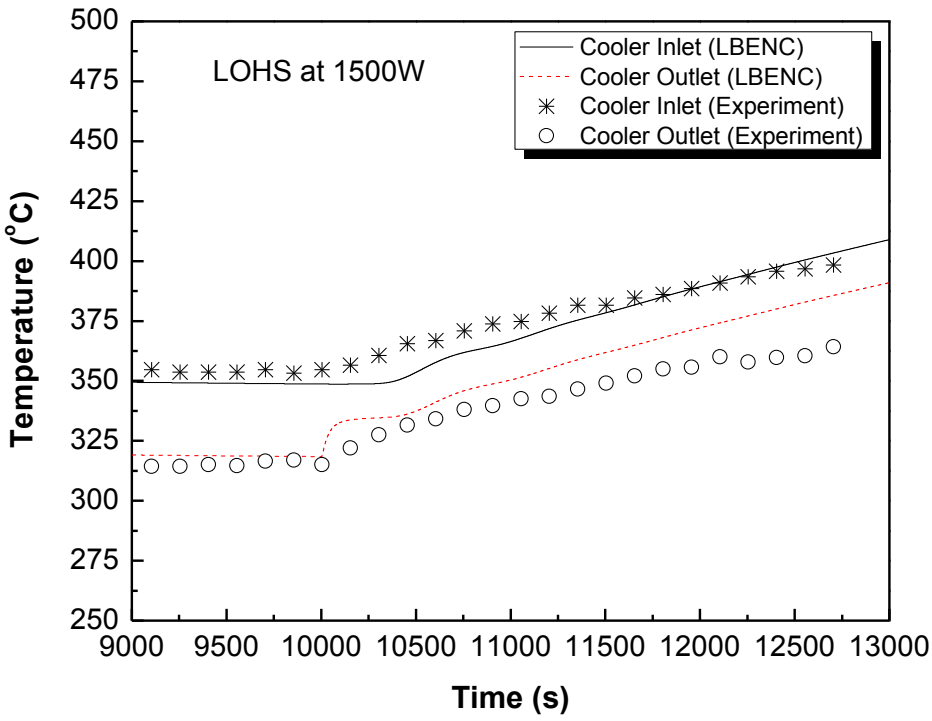

Figure 20. Cooler Inlet and outlet temperature variation in LOHS transient and its comparison with LeBENC

7.2.3 Heater trip

As explained earlier molten nitrate salt will be heated by concentrating solar rays is solar receiver for extracting solar thermal energy. During night and cloudy weather the solar heating is not possible, in that scenario the consequences of sudden non-availability of heat source is simulated using heater trip transient.

This transient was realized by setting the main heater power to zero value from steady state at some power. Initial conditions for this transient are as follows: loop was in steady state at 2000W power, secondary side air flow rate was maintained at 0.02kg/s. The start of the heater trip was simulated at 10000s. At this time the main heater power was set back to zero value from 2000W. As shown in Fig. 22 at the start of the transient, heater outlet temperature decreases rapidly and came closer to the heater inlet temperature due to the loss of heat source. This temperature drop was accomplished quickly and the inlet and outlet temperature of the heater then decreased together. Temperature drop in cooler inlet and outlet temperature can also be seen from Fig. 23.

In this case the temperature difference between cooler inlet and cooler outlet was initially decreased and then maintained a constant significant difference.

LeBENC results have also been compared with experimental data and found that the rate of decrease of temperature in LeBENC simulation is higher than that seen in experiment. This can be justified by explaining the geometry of MSNCL modeled in LeBENC. An expansion tank has been provided at the top of vertical cold leg in the loop (Fig. 1). It has a considerable volume of salt in comparison to main loop piping. Expansion tank has not been modeled in LeBENC. During heater trip experiment it was expected that the heat is transferred from the expansion tank to the loop piping causing slower temperature decrease rate than the LeBENC prediction.

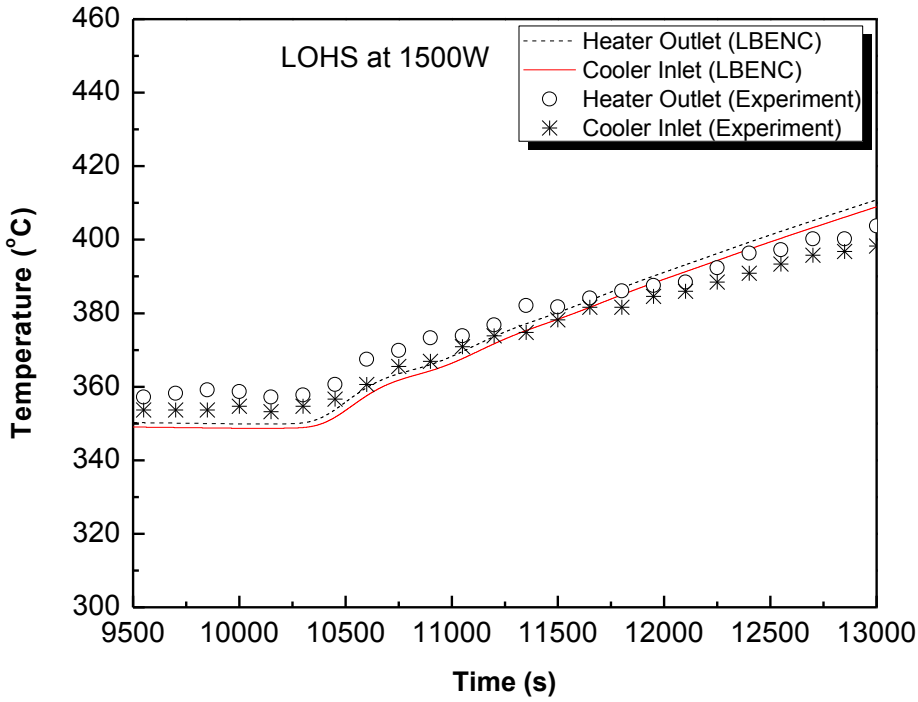

Figure 21. Heater outlet and Cooler Inlet temperature variation in LOHS transient and its comparison with LeBENC

8. CONCLUDING REMARKS

In this report literature survey of different molten salts proposed for solar power tower systems and high temperature reactor systems have been carried out. Design of Molten Salt Natural Circulation Loop (MSNCL) has been described. Steady state and transient experiments

concerned with the safety issues in designing solar power tower systems have been discussed and results for the same experiments have been presented. In addition to the experimental results, post-test calculations using the LeBENC code have been presented in order to demonstrate the value of the experimental results for code validation, which is an important step in ensuring the accuracy of the safety analysis of molten nitrate salt based solar power tower systems.

The following conclusions may be drawn, based on the experimental results:

- The Molten Salt Natural Circulation Loop (MSNCL) is well controlled and thermal hydraulic conditions for transient tests can be adjusted properly. It has been proved that it has a good capability to perform transient experiments.
- For the transient loss of heat sink, the temperature increases first from the cooler outlet, then to the downstream and finally in the whole loop. So, the temperature keeps going up if no protective measures are taken to mitigate the transient.
- Temperature drop is first seen at heater outlet in case of heater trip transient. Temperature difference across the heater suddenly decreases at initiation of startup and then average temperature of whole loop decreases.
- If there is a change in main heater power from steady state, the loop attains a new steady state according to the new applied power.

In general, transient experiments given a good demonstration of the safety performance of a molten nitrate salt based solar power tower systems, which is favored by its significant natural circulation.

After comparing the LeBENC results and steady state correlation with the experimental data the following conclusion are derived:

- The comparison of the LeBENC results with the experimental data for the transients shows good agreement for molten salt temperatures except the heater trip transient. The rate of decrease of temperature in LeBENC simulation is higher than that seen in experiment in case of heater trip transient which may match with experimental data by modeling the expansion tank.
- Experimental results are demonstrated over a wide range of different steady state and transient experiment using steady state correlation and LeBENC code.

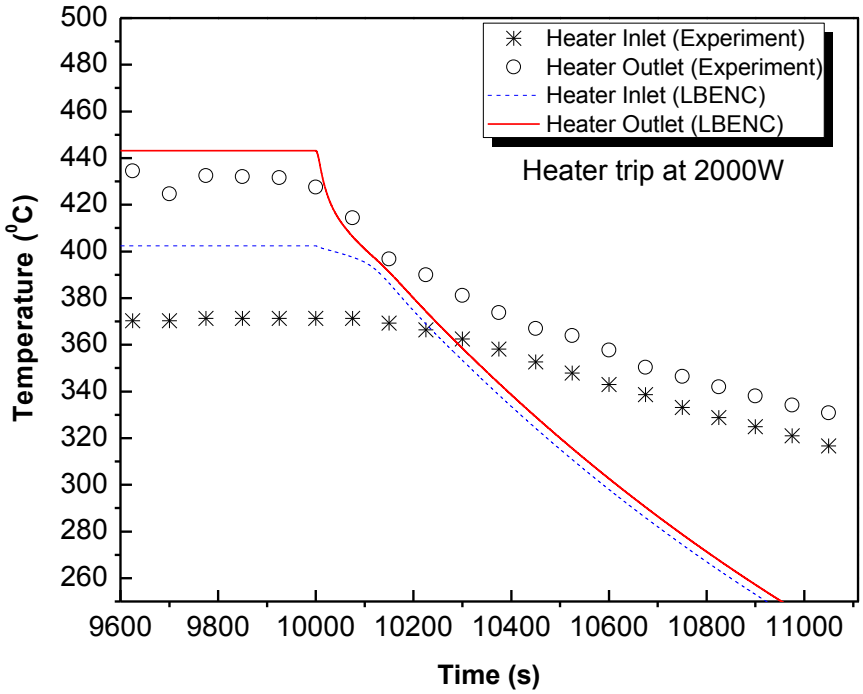

Figure 22. Heater outlet and Heater Inlet temperature variation in Heater trip transient and its comparison with LeBENC

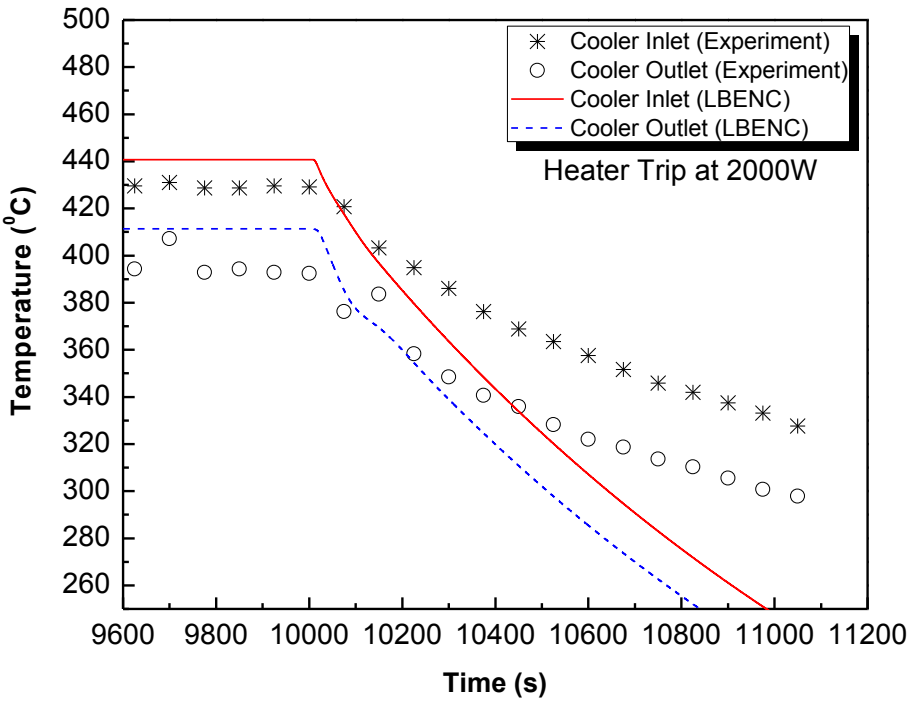

Figure 23. Cooler outlet and Cooler Inlet temperature variation in Heater trip transient and its comparison with LeBENC.

- Finally the comparison of LeBENC results with the experimental data indicates that the results of the steady state and transient experiments obtained in MSNCL can be reproduced using LeBENC code with good accuracy.

REFERENCE

[1] Survey of thermal storage for parabolic trough power plants, National Renewable Energy Laboratory, September 2000.

[2] R. W. Mar, J. C. Swearengen, Material Issues In Solar Thermal Energy Systems, Solar Energy Materials 5 (1981) 37-53.

[3] H. W. Hoffman and J. Lones, Forced convection heat transfer in circular tubes containing LiF-NaF-KF eutectic, ORNL-1777, Reactor-Research and Power, February 1, 1955.

[4] M.D. Silverman, W.R. Huntley, H.E. Robertson, Heat transfer measurement in a forced convection loop with two molten fluoride salt, ORNL/TM-5335, October 1976.

[5] D. Kearney , B. Kelly, U. Herrmann , R. Cable , J. Pacheco, R. Mahoney, H. Price, D. Blake, P. Nava, N. Potrovitza, Engineering aspects of molten salt heat transfer fluid in a trough solar field, Energy 29 (2004) 861–870.

[6] Robert W. Bradshaw& Nathan P. Siegel, Molten Nitrate salt development for thermal energy storage in parabolic trough solar power system, August 10-14, 2008, Jacksonville, Florida USA.

[7] Wu Yu-ting , Liu Bin, Ma Chong-fang, Guo Hang, Convective heat transfer in laminar-turbulent transition region with molten salt in a circular tube, Experimental Thermal and Fluid Science 33 (2009) 1128–1132.

[8] Liu Bin, Wu Yu-ting , Ma Chong-fang, Ye Meng, Guo Hang, Turbulent convective heat transfer with molten salt in a circular pipe, International Communications in Heat and Mass Transfer 36 (2009) 912–916.

[9] Marcello V. Di., Cammi A., Luzzi L., Analysis of Thermal Hydraulic Behavior of the Molten Salt Nuclear Fuel, International conference on Nuclear Energy for New Europe, September 8-11, 2008.

[10] Luke C. Olson , James W. Ambrosek, Kumar Sridharan, Mark H. Anderson, Todd R. Allen, Materials corrosion in molten LiF–NaF–KF salt, Journal of Fluorine Chemistry 130 (2009) 67–73.

[11] Kaiser J. R., DeVAN J. H., Lawrence E. J., Compatibility of molten salts with type 316 stainless steel and lithium, Journal of Nuclear Materials, 85 & 86 (1979) 295-298.

[12] Baraka A., Baraka R.M.S., Abdel-Razik A., The corrosion behavior of Nickel in molten $NaNO_3$-KNO_3 eutectic, Journal of Surface Technology, 26 (1985) 199-206.

[13] Goods S.H., Mechanical Properties of Low alloy Steel in Molten Nitrate Salt Environment, Metallurgical transactions A, Volume 16A, June 1985, 1031-1041

[14] Vijayan P.K., Sharma M., Saha D., Steady-state and stability characteristics of single-phase natural circulation in a rectangular loop with different heater and cooler orientations, Experimental Thermal and Fluid Science, Vol. 31, 925-945 (2007).

[15] Zvirin Y., A review of natural circulation loops in PWR and other systems, Nuclear. Engineering Design, 67 pp. 203-225 (1981).

[16] Welander P., On the oscillatory instability of a differentially heated fluid loop, J. Fluid Mechanics, vol. 29-1, pp. 17-30 (1967).

[17] P. F. Tortorelli, J. H. DeVan, Thermal-convection-loop study of the corrosion of Fe-Ni-Cr alloys by molten NaNO3–KNO3, ORNL/TM-8298, Dist. Category UC-95, December 1982.

[18] P.K Vijayan, Experimental and numerical investigations on the nature of the unstable oscillatory flow in a single-phase natural circulation loop, XVII National and VI ISHMT/ASME Heat and Mass Transfer Conference, IGCAR, Kalpakkam, Jan 5-7 HMT-2004-C100, pp 600-606.

[19] P.K. Vijayan, V.K. Bhojwani, M.H. Bade, M. Sharma., A.K. Nayak., D. Saha and R.K Sinha, Investigations on the effect of heater and cooler orientation on the steady state, transient and stability behaviour of single phase natural circulation in a rectangular loop, BARC/2001/E/034, 2001.

[20] P.K Vijayan, Experimental observation on the general trends of the steady state and stability behaviour of single-phase natural circulation loops, Nuclear Engineering and Design, 215, 2002, pp 139-152.

[21] www.specialmetals.com, INCONEL alloy 625 and SS316.

LIST OF ABBREVIATIONS

ASME	American Society of Mechanical Engineers
HHHC	Horizontal Heater and Horizontal Cooler
HHVC	Horizontal Heater and Vertical Cooler
LMTD	Logarithmic Mean Temperature Difference
NB	Nominal Bore
SORF	Slip-On-Raised Face
VHHC	Vertical Heater and Horizontal Cooler
VHVC	Vertical Heater and Vertical Cooler

NOMENCLATURE

A	Flow area, m^2
b	Exponent in the friction factor equation
C_p	Specific heat at constant pressure, J / kgK
D_H	Hydraulic Diameter, m
f	Friction factor
g	Acceleration due to gravity, m / s^2
Gr_m	Modified Grashof number, $D^3 \rho^2 \beta g \Delta T_r / \mu^2$
H	Elevation difference between heater and cooler, m
h	Heat transfer coefficient, $W / m^2 K$
I	Current, A
K	Loss coefficient
k	Thermal conductivity, W / mK
L	Length, m
Nu	Nusselt number, hD / k
p	Constant in friction factor equation
Pr	Prandtl number, $\mu C_p / k$
Δp	Pressure drop, Pa
Q	total heat input rate, W
Q_h	Heater Power, W
r	Redial co-ordinate direction
Re	Reynolds number, $\rho v D_H / \mu$
s	Co-ordinate direction around the loop

t	Time, s
ΔT_r	reference temperature difference, $\left(QH / A\mu C_p\right)$, K
T	Temperature, ^0C
U	Overall heat transfer coefficient, W / m^2K
v	Velocity, m/s
W	Mass flow rate, kg / s

GREEK SYMBOLS

α	Diffusion coefficient, m^2/s
β	Coefficient of thermal expansion, 1/K
ρ	Density, kg/m^3
μ	Dynamic viscosity, Pa.s
ζ	Flow Resistance
γ	Specific gravity

SUBSCRIPTS

b	Bulk
DF	Driving force
e	Equivalent
eff	Effective
i	Inlet
j	Nodes along the length
n	time step
o	Outside
ss	Steady state
t	Total
w	Wall
lam	Laminar Flow
s	Secondary side

APPENDIX-1

Temperature dependent properties of Molten Nitrate Salt

The temperature dependent properties of molten nitrate salt, a eutectic mixture of $NaNO_3$ and KNO_3 in 60:40 ratio is given in Table A-1.1:

Table A-1.1 [1]

Temperature (^{0}C)	Specific Heat (J/kgK)	Density (kg/m^3)	Thermal conductivity (W/mK)	Viscosity (Pa s)
227	1486.499	1945.628	0.486356	5.500E-03
277	1495.089	1913.828	0.496126	3.839E-03
327	1503.679	1882.028	0.505896	2.707E-03
377	1512.269	1850.228	0.515666	1.992E-03
427	1520.859	1818.428	0.525436	1.583E-03
477	1529.449	1786.628	0.535206	1.372E-03
527	1538.039	1754.828	0.544976	1.246E-03
577	1546.629	1723.028	0.554746	1.096E-03
627	1555.219	1691.228	0.564516	8.098E-04

The graphical representation of these properties is shown below:

Density:

$$\rho = 2090.0 - 0.636T \quad \text{(A-1.1)}$$

Specific heat:

$$C_p = 1447.5 + 0.1718T \quad \text{(A-1.2)}$$

Viscosity:

$$\mu = 93.03T^{-1.8} \quad \text{(A-1.3)}$$

Thermal conductivity:

$$k = 0.442 + 0.0002T \quad \text{(A-1.4)}$$

1) **Density vs. Temperature**

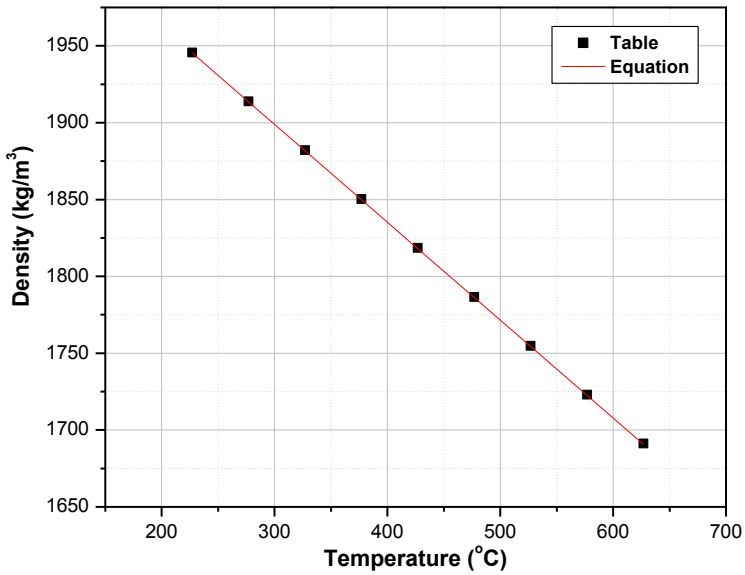

Figure A-1.1 Density vs. Temperature

2) **Specific heat vs. Temperature**

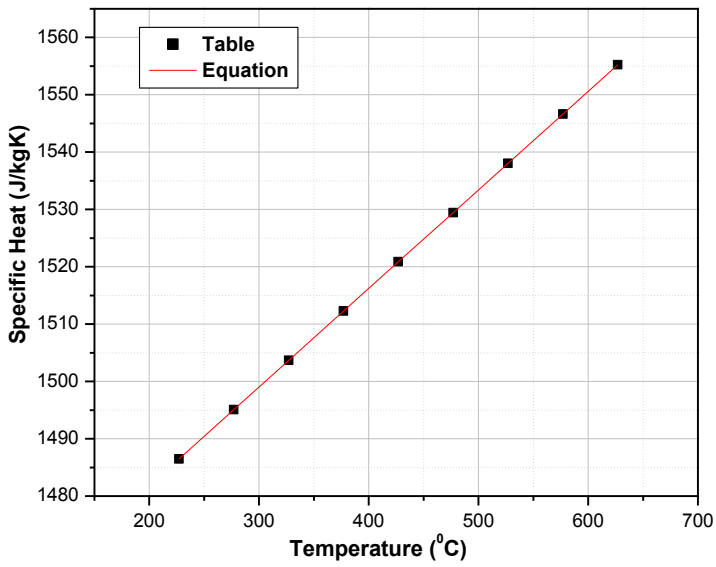

Figure A-1.2 Specific heat vs. Temperature

3) Thermal Conductivity vs. Temperature

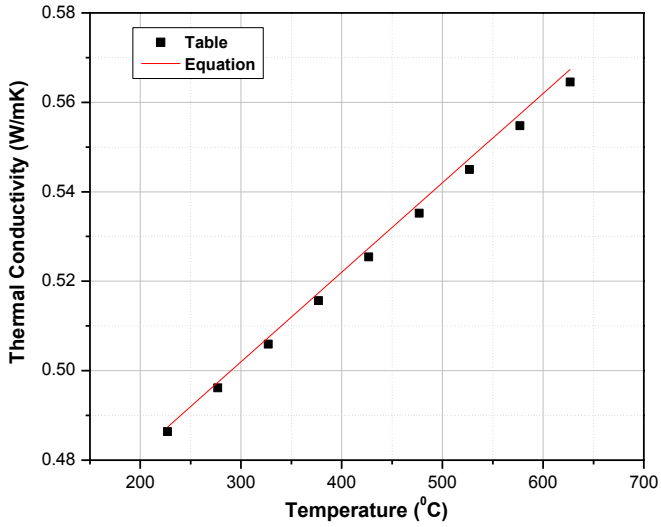

Figure A-1.3 Thermal conductivity vs. Temperature

4) Viscosity vs. Temperature

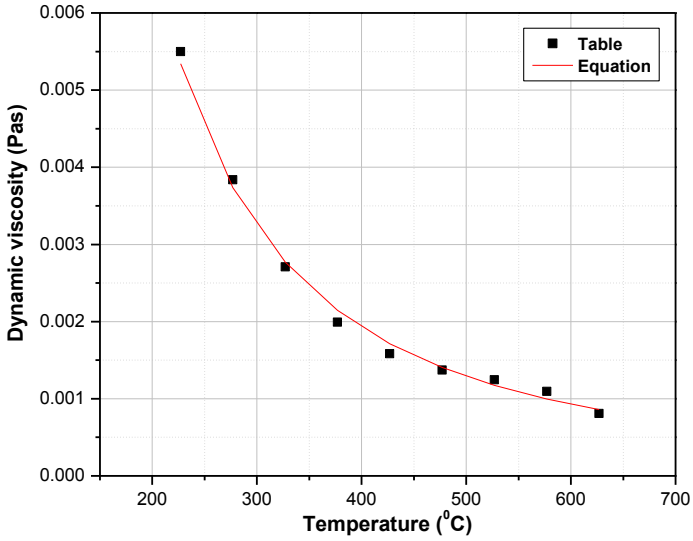

Figure A-1.4 Viscosity vs. Temperature

REFERENCE

[1] Solar Power Tower Design Basis Document, Revision Zero, Report No. SAND-2001#2100

APPENDIX-2

Fire Load inside the Molten Salt Natural Circulation Loop (MSNCL) Cabin

1. List of Combustible material inside the Cabin and their Calorific value

Sr. No.	Combustible material	Category	Calorific Value [1] (Kcal/kg)	Amount (kg)	Total Heat (Kcal)
1	Teflon wires	PVC Cable Insulation	4298	10	42980
2	PVC Conduit	PVC	11000	2	22000
3	Electrical switches	PVC	11000	2	22000
4	Acrylic	Plastic	11000	12	132000
5	Oil Paint	Oil Paint	10510	2	21020

2. Fire Load

The floor area of the cabin = (2.5 X 3.6) = 9 m^2

Total Heat = (42980+22000+22000+132000+21020) = 240000 Kcal

Total Fire Load = (240000/9) = 26667 Kcal/m^2

3. Categorization of Area [1]

Sr. No.	Categorization of Area related to Fire Hazard	Range Fire load (Kcal/m^2)
1	Low Hazard (LH)	< 2,75,000
2	Ordinary Hazard (OH)	2,75,000 to 5,50,000
3	High Hazard (HH)	>5,50,000

- ✓ **As per the categorization of Fire Hazard area on the basis of Fire load, the MSNCL area comes to the Low Hazard (Fire Load in MSNCL 26667 << 2,75,000 LH) group.**

REFERENCE

[1] Gupta, R.S., *A Handbook of Fire Technology*, Orient Longman Pvt. Ltd., 2005 Reprint.

APPENDIX-3

Process Design of Various Components

The design of various process equipments such as: Cooler, Elbow and Tee are explained in this section.

A-3.1 Cooler

Pipe in pipe type cooler is designed for molten salt test facility (Fig. A-3.1). Air is used as a secondary side coolant. Calculation is performed for size of the cooler. Air jacketing is done through a 4" pipe over a ½" main line pipe. Forced circulation of air is maintained with the help of a blower having 1000cfm capacity.

Salt side:

Selected primary side line size is ½" (15NB) SCH80 pipe having

Inner Diameter (ID) = 13.6mm

Outer Diameter (OD) = 21.3mm

Initial condition of the salt entering to the cooler $T_i = 300^oC$ & Q=1000W

For uniform heat flux applied on the heater, the steady state natural circulation flow rate for VHHC orientation has been calculated by equation:

$$W = \left[\frac{2\beta g \rho^2 D^{1+b} A^{2-b} Q_h H}{p \mu^b C_p L} \right]^{\frac{1}{3-b}} \tag{A-3.1}$$

With the help of above written equation, the steady state natural circulation flow rate for different power has been calculated and listed in table 6.1

With this approximation of flow rate, heat transfer coefficient of salt side is calculated as:

$$Q = WC_P \Delta T$$

$$W = 0.01772 kg/s$$

Table A-3.1 Steady state natural circulation flow rate at different power

Power Q (W)	Steady state flow rate W (kg/s)
200	0.007925
400	0.011207
600	0.013726
800	0.015849
1000	0.01772

Reynolds number of the flowing salt is given by

$$\mathrm{Re} = \frac{\rho v D_H}{\mu} = 757.88 \quad \text{(A-3.2)}$$

As the Reynolds number corresponding to salt, flowing in primary side, comes in laminar region, the Nusselt number for constant heat flux condition is fixed to 4.36. [17] and hence the heat transfer coefficient for salt side is given as:

$$Nu = \frac{h_i D_H}{k} = 4.36 \quad \text{(A3.3)}$$

$$h_i = \frac{Nu * k}{D_H} = 155.98 \text{ W/m}^2\text{-K} \quad \text{(A3.4)}$$

Air side:

Selected Secondary side line size is 4" (100NB) SCH40 pipe having

Inner Diameter (ID) = 102.26mm

and Outer Diameter (OD) = 114.3mm

Initial condition of the salt entering to the cooler $T_i = 30^oC$ & W=700cfm, Q=1000W

(From Heat Balance)

$$Q = WC_P\Delta T$$

Hence the outlet air temperature comes as:

T_o=50^{o}C

For the assumed flow rate the Reynolds Number is given by:

$$\mathrm{Re} = \frac{\rho v D_H}{\mu} = 1.5\mathrm{E}5$$

The air side flow lies in turbulent region hence Dittus-Bolter correlation for heat transfer is applicable:

$$Nu = 0.023\,\mathrm{Re}^{0.8}\,\mathrm{Pr}^{0.3} \qquad \text{(A-3.5)}$$

Using the thermophysical properties of air the Nusselt number is given as:

$$Nu = 292 \qquad \text{(A-3.6)}$$

And hence the heat transfer coefficient for secondary side is given by:

$$h_o = \frac{Nu * k}{D_H} = 98.915\mathrm{W/m^2\text{-}K} \qquad \text{(A-3.7}$$

The overall heat transfer coefficient is calculated by formula:

$$U_o = \frac{1}{\{A_o/(A_i h_i) + A_o f_i + d_o * \ln(d_o/d_i)/2k + f_o + h_o\}} \qquad \text{(A-3.8)}$$

$$U_o = 48.51\frac{W}{m^2 K} \qquad \text{(A-3.9)}$$

Where f_i and f_o are Fouling factors for primary and secondary side respectively.

Considering counter flow current direction the logarithmic mean temperature difference (LMTD) is calculated as:

$$\Delta T_{LMTD} = \frac{\Delta T_1 - \Delta T_2}{log_e(\Delta T_1/\Delta T_2)} = 278.92527^o\mathrm{C} \qquad \text{(A-3.10)}$$

ΔT_1=temperature difference of primary and secondary side fluids at inlet

ΔT_2 =temperature difference of primary and secondary side fluids at outlet

Now the required heat transfer area is calculated by:

$$Q = U_0 A_0 \Delta T_{LMTD} \quad \text{(A-3.11)}$$

$$A_0 = 0.07314 m^2 = \pi D_0 L$$

And hence the length of the cooler comes as:

$$L = 1.058 m \quad \text{(A-3.12}$$

Figure A-3.1 Cooler

A-3.2 Elbow

Flow resistance coefficient of the ½" (15NB) socket weld elbow is calculated which are used in molten salt test facility. Ratio of radius of curvature to hydraulic diameter for standard 15NB socket weld elbow is given as:

R_o/D_H=31.7/15=2.1133mm (A-3.13)

Figure A-3.2 Photograph of socket weld elbow

Flow resistance for smooth bends and rough walls having $Ro/D_H > 1.5$ and for Re greater or less than $2*10^5$ is given as [20]:

$$\zeta = \frac{\Delta H}{\frac{\gamma w_0^{\,2}}{2g}} = k_{\Delta} k_{\mathrm{Re}} \zeta_l + \zeta_{fr} \qquad \text{(A-3.14)}$$

Where

ΔH = Pressure loss in, kg/m^2

w_0 =stream velocity, m/s

γ =Specific gravity of the flowing medium, kg/m^3

ζ_l =coefficient of local fluid resistance

ζ_{fr} = friction coefficient

Friction coefficient is given as:

$\zeta_{fr} = 0.00035 \frac{R_o}{D_H} \delta^0$, where δ^0 = angle of the elbow in degree. (A-3.15)

Therefore for 90^0 elbow, the friction coefficient ζ_{fr} =0.066

Coefficient of local fluid resistance, $\zeta_l = A_1 B_1 C_1$

For 90^0 elbow A_1 =1.0, B_1 =0.15, C_1= 1.00

This results in local loss coefficient as $\zeta_l = 0.15$

The value of k_Δ =1.00 and of $k_{\mathrm{Re}} = 64\lambda_{\mathrm{Re}}$ = 64*0.064=4.096, for Re=1000

Hence the value of flow resistance coefficient for ½" (15NB), 90^0 socket-weld elbow is given as:

$$\zeta = \frac{\Delta H}{\frac{\gamma w_0^{\,2}}{2g}} = k_\Delta k_{\mathrm{Re}} \zeta_l + \zeta_{fr} = 0.6144 + 0.066 = 0.6804 \qquad \text{(A-3.16)}$$

A table is provided for flow resistance coefficient, calculated for ½" (15NB), 90^0 socket-weld elbows with different Reynolds number.

Table A-3.2 Flow Resistance coefficient of elbow for different Reynolds Number

Reynolds Number (Re)	Flow resistance coefficient (ζ)
400	1.602
2000	0.565
3000	0.498
5000	0.432

A-3.3 Equal Tee

Flow resistance coefficient of the ½" (15NB) socket weld equal tee is calculated which are used in molten salt test facility.

Figure A-3.3 Photograph of socket weld equal tee

The flow resistance coefficient for symmetrical 90^0 Tee is given as [1] :

$$\zeta_{c,b} = \frac{\Delta H_b}{\frac{\gamma w_c^{\,2}}{2g}} = 1 + k\left(\frac{w_b}{w_c}\right)^2 \qquad \text{(A-3.17)}$$

Where $\zeta_{c,b}$ = resistance coefficient of the branch in terms of the velocity in terms of the velocity in common channel

w_c = velocity in the channel, m/s

w_b = velocity in the branch, m/s

And the value of k= 0.3, for welded tee.

The velocity relation between channel and branch of equal tee is given by:

$w_c = 2w_b$

Hence the resistance coefficient of ½" (15NB) socket weld equal tee is given as:

$$\zeta_{c,b} = 1 + k\left(\frac{w_b}{w_c}\right)^2 = 1 + 0.3\left(\frac{w_b}{2w_b}\right)^2 = 1.075 \qquad \text{(A-3.18)}$$

REFERENCE

[1] I.E. Idelchik, Handbook of Hydraulic Resistance.